Cell Membrane-Coated Magnetic Nanocubes with a Homotypic Targeting Ability Increase Intracellular Temperature due to ROS Scavenging and Act as a Versatile Theranostic

Cell membrane-coated magnetic nanocubes with a homotypic targeting ability increase intracellular temperature due to ROS scavenging and act as a versatile theranostic system for glioblastoma multiforme

Christos Tapeinos[a,†,], Francesca Tomatis[b,†], Matteo Battaglini[a,c], Aitor Larrañaga[d], Attilio Marino[a], Iker Aguirrezabal Telleria[e], Angelakeris Makis[f], Doriana Debellis[g], Filippo Drago[h] Francesca Brero[i], Paolo Arosio[j], Alessandro Lascialfari[j], Andrea Petretto[k], Edoardo Sinibaldi[l], Gianni Ciofani [a,b,*]*

[a]Smart Bio-Interfaces, Istituto Italiano di Tecnologia, 56025 Pontedera, Italy

[b]Department of Mechanical and Aerospace Engineering, Politecnico di Torino, 10129 Torino, Italy

[c]The Biorobotics Institute, Scuola Superiore Sant'Anna, 56025 Pontedera, Italy

[d]Department of Mining-Metallurgy Engineering and Materials Science & POLYMAT, University of the Basque Country, 48013 Bilbao, Spain

[e]Department of Chemical and Environmental Engineering, Engineering School of the University of the Basque Country (UPV/EHU), 48013 Bilbao, Spain

[f] Department of Physics, Aristotle University of Thessaloniki, 54124 Thessaloniki, Greece

[g]Electron microscopy facility, Istituto Italiano di Tecnologia, 16163 Genova, Italy

[h]Nanochemistry Department, Istituto Italiano di Tecnologia, Genova, 16163 Italy

[i]Department of Physics and INSTM, Università degli Studi di Pavia, 27100 Pavia, Italy

[j]Department of Physics and INSTM, Università degli Studi di Milano, 20133 Milano, Italy

[k]Core Facilities-Clinical Proteomics and Metabolomics Laboratory, IRCCS Istituto Giannina Gaslini, 16147 Genova, Italy

[l]Center for Micro-BioRobotics, Istituto Italiano di Tecnologia, 56025 Pontedera, Italy

† These authors equally contributed to this work

* Corresponding authors: christos.tapeinos@iit.it, gianni.ciofani@iit.it

Abstract

In this study, we synthesized hybrid nanocubes composed of magnetite (Fe_3O_4) and manganese dioxide (MnO_2), coated with U-251 MG cell-derived membranes (CM-NCubes). The CM-NCubes demonstrated a concentration-dependent oxygen generation (up to 15%), and, for the first time in literature, we showed an intracellular increase of temperature (4°C) due to the exothermic scavenging reaction of hydrogen peroxide (H_2O_2). Internalization studies demonstrated that the CM-NCubes were internalized much faster and at a higher extent by the homotypic U-251 MG cell line compared to other cerebral cell lines. The ability of the CM-NCubes to cross an in vitro model of the blood-brain barrier (BBB) was also assessed. The CM-NCubes showed the ability to respond to a static magnet and to accumulate in cells even under flowing conditions. Moreover, we demonstrated that 500 µg ml^{-1} of sorafenib-loaded and unloaded CM-NCubes are able to induce cell death by apoptosis in U-251 MG spheroids that were used as a tumor model, after their exposure to an alternating magnetic field (AMF). Finally, it was shown that the combination of sorafenib and AMF induces a higher enzymatic activity of caspase 3 and caspase 9, probably due to an increment in reactive oxygen species (ROS) by means of hyperthermia.

Keywords: cell membrane-coated nanocubes, glioblastoma, homotypic targeting, magnetic hyperthermia, theranostics

1. Introduction

According to the 2016 World Health Organization (WHO) classification of tumors, glioblastoma multiforme (GBM) is one of the most commonly diagnosed brain cancers. This neoplasia, characterized by astrocytic differentiation, is one of the most aggressive central nervous system malignancies, resulting in poor prognosis and low survival rates mostly due to its late diagnosis.[1] Current treatment strategies include tumor resection using combinatory adjuvant or neoadjuvant radiotherapy and chemotherapy, but they fail to successfully treat GBM due to various reasons, including the location and the pathophysiology of the tumor, the hypoxic microenvironment that has been proven to be related to the multidrug resistance (MDR) phenomenon,[2] and the blood-brain barrier (BBB), that hinders the efficient delivery of various anticancer drugs.[1b, 3]

Since surgical resection is not always feasible, and since chemotherapy and radiotherapy are at a greater extent palliative than curative exhibiting reduced effectiveness together with pronounced side-effects, novel methodological approaches are to be developed for the treatment of various brain cancers including glioblastoma. These methods make use of smart drug delivery systems (DDS) able to cross the BBB and to specifically target the diseased tissue. These nanovectors may be stimuli-responsive, and take advantage of the tumor microenvironment resulting in alterations of their morphological and/or physicochemical properties, depending on the biological, physical and/or chemical cues.[4]

One of the best-studied systems that make use of an external stimulus in order to kill cancer cells is represented by superparamagnetic iron oxide nanoparticles (SPIONs). SPIONs constitute an attractive therapeutic system for solid tumors, due to the fact that they i) present negligible cytotoxicity, ii) can be easily modified to target specific types of cancer, iii) have the ability to encapsulate a variety of drugs, iv) in principle can be magnetically guided

to the site of interest, v) can be used as diagnostics agent due to their ability to act as contrast agents in MRI, and vi) eventually they can kill cancer cells through magnetic fluid hyperthermia under the influence of an alternating magnetic field. All of these characteristics render SPIONs promising candidates for non-invasive cancer treatment.[4c, 5]

Another type of inorganic nanoparticles that started to be used in the latest 5 years for the treatment of cancer and other inflammatory diseases is represented by manganese dioxide (MnO_2) nanoparticles. MnO_2 nanoparticles have the ability to scavenge hydrogen peroxide (H_2O_2) by producing oxygen.[2, 6] This combination leads to a reduction of oxidative stress that has been related to tumor cell survival, proliferation, and angiogenesis,[7] as well as with the regulation of the hypoxia-inducible factor-1α (HIF-1α) due to oxygen generation, that has also been associated to neovascularization, metastasis, and other phenomena. [8]

Despite both SPIONs and MnO_2 nanoparticles can act as therapeutic enhancers, they are still not so effective to completely eliminate a tumor. Aiming at further enhancing their therapeutic activity, these nanoparticles can be loaded with chemotherapeutic agents like temozolomide (TMZ), and through a combinatory effect to increase their efficacy. Despite the fact that the TMZ is the most used FDA-approved chemotherapeutic agent in glioblastoma, sorafenib (SOR), a tyrosine protein kinase inhibitor (TPKI), has been also used in phase I and II clinical trials with and without TMZ aiming at treating glioblastoma, among other types of cancer[9].

A successful delivery system is also characterized by its ability to safely deliver its encapsulated therapeutic compound to a specific tissue. In order to achieve this aim, the surface of the DDS can be functionalized with targeting moieties able to bind specific receptors that are over-expressed in cancer cells. In spite of the fact that several functionalization techniques have been used over the years, the amount of therapeutics that

can cross the BBB is still very low.[10] This phenomenon can be attributed to the strong endothelial cell tight junctions of the BBB that make central nervous system inaccessible,[3] as well as to the excretion of the DDS from the circulatory system through opsonization.[11] Aiming at overcoming these limitations, cell membrane coatings are starting to be used as a more biomimetic approach for the fabrication of smart DDS. The cell membrane provides stealth abilities to the coated DDS inhibiting its uptake by macrophages, and in many cases can lead to a homotypic cell targeting, demonstrating specific targeting ability.[12]

Herein, taking into consideration the limitations that the current treatment and delivery strategies present, and acknowledging the complex milieu of cancer microenvironment, we hypothesized that a multi-functional approach will lead to a bemeficiary therapeutic outcome. In view of this, we fabricated nanoparticles based on an inorganic core composed of magnetite (Fe_3O_4) and MnO_2 in the form of nanocubes (NCubes), which were then coated with U-251 MG cell-derived membranes. These NCubes were able to scavenge an excess of hydrogen peroxide (H_2O_2), and at the same time to increase O_2 levels in a concentration-dependent manner, due to the MnO_2 component, while the Fe_3O_4 presence guaranteed the ferromagnetic character, thus, the guidance by external static magnetic field together with magnetic particle hyperthermia efficiency . Furthermore, the synthesized inorganic NCubes were able to induce apoptosis and necrosis in U-251 MG spheroids through hyperthermia and demonstrated an enhanced apoptotic effect when loaded with the chemotherapy drug sorafenib. The CM-NCubes were also tested for their ability to act as Magnetic Resonance Imaging (MRI) contrast agents, and it was found that their relaxivity r_2 was higher than that one of commercial contrast agent Endorem® withdrawn from the market in the last years.[13] Furthermore, we demonstrated that the CM-NCubes were able to cross an *in vitro* model of the BBB and that the cell membrane coating resulted into a higher internalization owing to a

homotypic binding to U-251 MG cells. Aiming at fully exploiting the magnetic component of the CM-NCubes, we assessed the combinational effect of a static magnetic field in close proximity to a dynamic microfluidic BBB *in vitro* model that consisted of an upper chamber seeded with bEnd.3 cells and a lower static compartment seeded with U-251 MG cells. [14] The results of this experiment demonstrated that under the effect of the static magnetic field the internalization and the subsequent crossing of the CM-NCubes through the bEnd.3 cell layer is significantly faster.

2. Results and discussion

2.1 Morphological and physicochemical characterization

NCubes were synthesized using a simple one-pot procedure as described below, and a thorough physicochemical analysis was performed. The coating of the plain NCubes with cell membrane-derived lipids was performed aiming at the fabrication a multifunctional system, as presented in **Fig. 1A**. The first investigation that has been carried out was transmission electron microscopy (TEM) (**Fig. 1B**), that allowed the observation of the formation of cell membrane coated nanocubes with an average diameter of 20 ± 3 nm.

Infrared spectroscopy (**Fig. 1C)** of both uncoated (NCubes) and coated nanocubes (CM-NCubes) demonstrated the successful presence of Fe-O and Mn-O bonds in the range 500 – 700 cm^{-1} and 650 – 860 cm^{-1}, respectively. It has to be noted that the vibrations of the peaks ascribed to the bonds of 'metal-oxygen' are interfering each other, resulting into a small shift in comparison to other reported values in the literature. [15] The broad peak at approximately 1750 cm^{-1} that can be seen only in the CM-NCubes spectrum can be attributed to the C-N and C=O vibrations of the cell membranes; the same applies for the peaks around 2800 cm^{-1}, which are attributed to the C-H vibration. The small peak that is observed also around at

2800 cm^{-1} in NCubes can be probably attributed to an impurity since during the synthetic procedure, no organic compounds are used.

In order to assess the crystalline structure of the synthesized NCubes and CM-NCubes, we performed X-ray diffraction analysis (XRD) and the results that are presented in **Fig. 1D** demonstrate that both NCubes and CM-NCubes present the spinel structure of magnetite. In addition to this, the peak at 2θ = 38.6° is attributed to the MnO_2, as it can also be seen from the XRD graph and the detailed XRD analysis presented in the supporting information (**Fig. S2**, **Fig. S3**, **Table S1,** and **S2**, ESI†), suggesting that we have both the crystalline structures in the synthesized NCubes and in the CM-NCubes. Using the Scherrer's equation $B = K \cdot \lambda / L \cdot \cos\theta'$ (where *K* is a dimensionless shape factor and is equal to 0.94, λ is the wavelength of the electron source and is equal to 0.154 nm, and *L* is the full width at the half maximum of a chosen peak), we were also able to calculate the crystallite size of the CM-NCubes, which was found to be 18.3 ± 2.9 nm, which is in very close agreement with the TEM results.

When thermogravimetric analysis (TGA) (**Fig. 1E)** was performed on the plain NCubes no weight reduction was observed, whilst a reduction that started above 100°C, and that can be attributed to the degradation of the cell membranes, could be observed for the CM-NCubes. The remaining percentage of the CM-NCubes at 600°C was approximately 88%, indirectly demonstrating that the cell membrane surrounding the CM-NCubes comprises 12% of the total weight.

X-ray photoelectron spectroscopy (XPS) was also used as a complementary technique to prove the coating of the NCubes with cell membranes, and the results are presented in **Fig. 1F**. Although both the spectra (NCubes and CM-NCubes) present C and N, it can be observed (see also **Table S3** and **Table S4**, ESI†) that the percentages of these elements for the CM-NCubes are higher with respect to the control, suggesting the presence of a cell membrane

layer. Moreover, according to the data derived from the deconvolution of the XPS peak of iron, it was calculated that the ratio of Fe(3+) / Fe(2+) is equal to 2, a value that is in agreement with other studies[16].

Inductively coupled plasma - optical emission spectrometry was also performed aiming to exactly calculate the percentages of Fe and Mn, as well as to further verify the presence of a cell membrane. The results for the uncoated NCubes showed a concentration of 67.2% Fe and 6.1% Mn, while for the CM-NCubes showed 62.5% Fe, 5.86% Mn and 0.22% P, suggesting the presence of a phospholipidic layer. Furthermore, the reduced value of Fe/Mn ratio on the surface of NCubes, which is 5.5/1 calculated by XPS, with respect to the ratio of the whole structure (11/1) as it can be calculated from the inductively coupled plasma optical emission spectroscopy (ICP-OES), shows that the percentage of Mn is higher on the surface of the CM-NCubes.

In order to visualize the location of the elements on the CM-NCubes, as well as to quantify these elements, we performed electron dispersive X-ray analysis. The results presented in **Fig. 1G-1 – Fig. 1G-6** are related to the CM-NCubes, and demonstrate the homogeneous distribution of the elements on a single nanocube, further supporting XPS and ICP results outlining the presence of a cell membrane layer on the CM-NCubes. We would like to highlight that we tried to visualize the cell membrane coating using transmission electron microscopy, but this method was proved to be unsuccessful, probably due to the low thickness of the coating. Nevertheless, the electron dispersive X-ray analysis performed on a sample of plain NCubes (**Fig. S1**, ESI†) did not show any carbon or phosphorus content, contrarily to analysis performed on CM-NCubes (**Fig. 1 G1-G6**): an evidence that further supports the presence of an organic coating on the CM-NCubes. A complementary method that we used to verify the presence of a cell membrane component around the particles was

the sodium dodecyl sulfate-polyacrylamide gel electrophoresis (SDS-PAGE). As it can be observed in **Fig.S3-A**, the CM-NCubes samples (at different concentrations: 125, 250 and 500 μg ml^{-1}; **Fig. S4 - Lanes 1, 2 & 3**, ESI^{+}) present molecular weight bands in the range of 15 – 25 kDa. As the concentration of the CM-NCubes increases, darker bands that correspond to higher amounts of cell membrane proteins are observed. On the other hand, no band can be observed for the uncoated NCubes sample (**Fig. S4 - Lanes 4 & 5**, ESI^{+}), thus proving the presence of cell membrane material on the CM-NCubes.

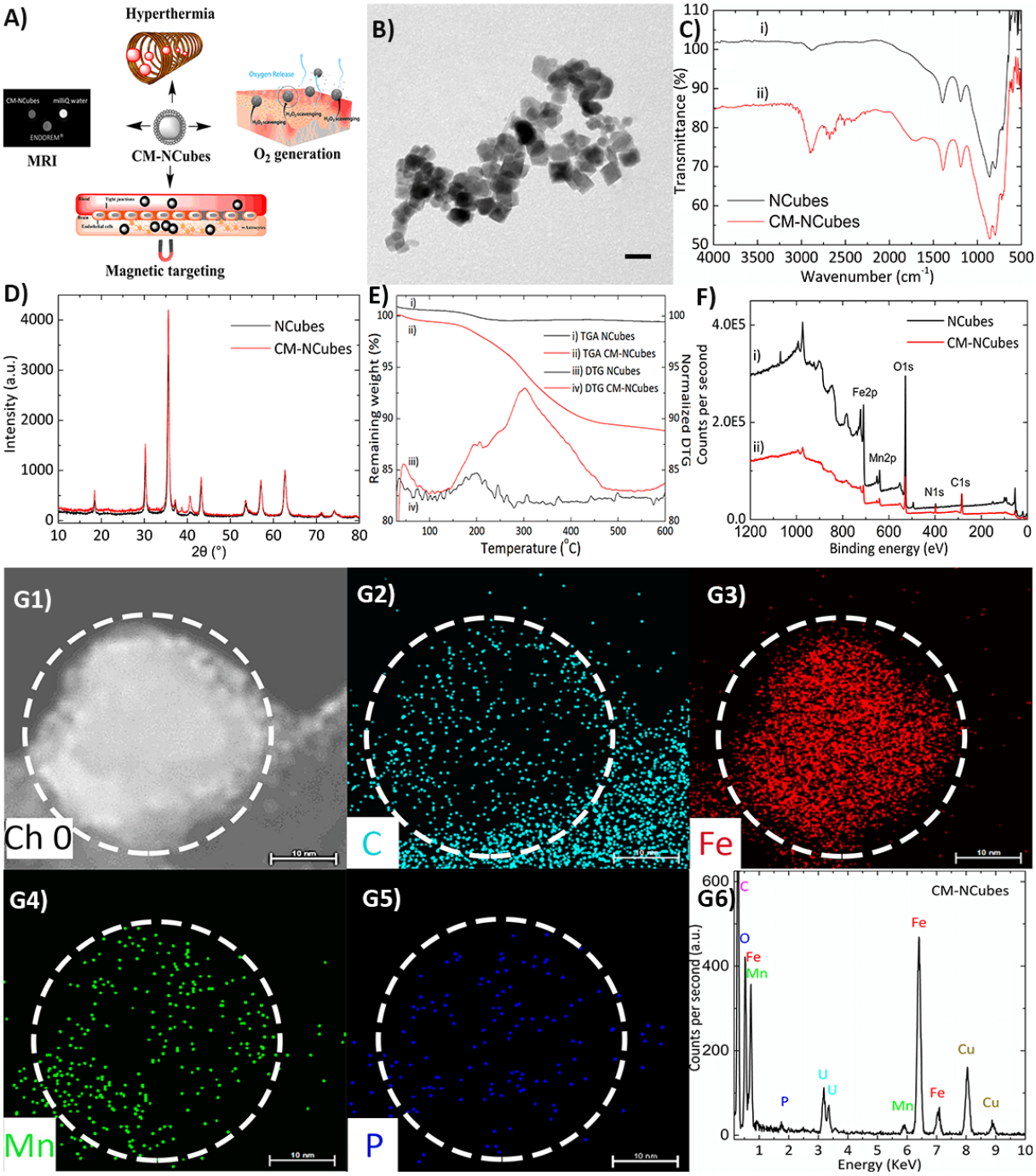

Figure 1. Synthesis and characterization of MnO_2-dopped iron oxide nanocubes (NCubes) and of cell membrane-coated NCubes (CM-NCubes). A) Schematic representation demonstrating the potential applications of the synthesized CM-NCubes; B) transmission electron microscopy image showing CM-NCubes (scale bar: 20 nm); C) Fourier-transformed infrared spectroscopy of NCubes and CM-NCubes, showing the presence of extra peaks in the range 1500 - 3000 cm^{-1} (spectrum *ii*) that can be attributed to the successful coating with the cell membrane; D) X-ray diffraction pattern of CM-NCubes presenting the crystalline spinel structure of Fe_3O_4 as well as the presence of Mn (peak at 2θ =38.6°; E) thermogravimetric analysis spectra

showing the weight loss and the first derivative of the weight loss; the decrease of weight by 12 % in the CM-NCubes sample is attributed to the decomposition of the cell membrane coating (temperature range 100-500 °C); F) X-ray photoelectron spectrum presenting the elements (C, N, O, Mn and Fe) found on the surface of NCubes and of CM-NCubes; G1-G5) electron dispersive X-ray analysis and mapping of a single CM-NCubes showing the presence and the distribution of carbon (C), iron (Fe), phosphorus (P) and manganese (Mn), proving the presence of an organic coating (scale bar: 10 nm); G6) electron dispersive X-ray analysis spectrum showing all the elements present on the surface of CM-NCubes. Increase percentages of carbon, at the bottom right corner of the corresponding EDS image, are present due to the carbon film-coated TEM grid. In addition, Cu and U present in the EDS spectrum are attributed to the TEM grid as well as to the staining of the CM-NCubes with uranyl acetate.

Lanes 6 and 7 and the ESI^{+} correspond to a standard molecular weight marker (Sigma Aldrich) and the corresponding ladder. Finally, mass spectroscopy was performed in order to verify the protein content on the surface of the CM-NCubes. Mass spectroscopy was used to characterize the protein content of both the raw product (extracted cell membrane) and the product adhering on the surface of the CM-NCubes. The results that are presented in **Fig. S4-B**, **Fig. S4-C** and **Fig S4-D**, ESI^{+}, demonstrate that same proteins are present in the two samples, suggesting that the coating procedure of the CM-NCubes does not alter the qualitative content of the cell proteins. Furthermore, some of the identified proteins, including basigin (BSG), cluster differentiation-44 (CD44), catenin beta 1 (CTNNB1), myosin light-chain kinase (MYLK), tight junction protein 1 (TJP1), endothelial growth factor (EGFR) and cluster differentiation-59 (CD59), that were found after the analysis of the MS data, have been shown to be present and overexpressed on the surface of glioblastoma cells, and this may be one of the reasons for the enhanced internalization of the CM-NCubes that is described later.

2.2 Stability studies and protein corona formation

It is well-known that the behavior of nanostructure-based drug delivery systems dramatically changes after their administration *in vivo* due to several reasons, which include their interaction with the proteins present in various body fluids, such as the blood and/or the cerebrospinal fluid. These interactions may affect the colloidal stability of the nanostructures, subsequently affecting their targeting and release abilities. In order to evaluate how well-known proteins in the blood and in the cerebrospinal fluid can affect the stability of the fabricated NCubes and CM-NCubes, we performed dynamic light scattering studies choosing as dispersants distilled water, Dulbecco's Modified Eagle Medium (DMEM), and artificial cerebrospinal fluid (aCSF). Distilled water was used as a reference for the evaluation of the colloidal stability since it does not contain any salts and/or supplements that may affect the hydrodynamic size and/or the polydispersity of both NCubes and CM-NCubes. DMEM with supplements was used in order to assess the behavior of the NCubes and CM-NCubes concerning *in vitro* studies, while aCSF was used in order to assess the behavior of the CM-NCubes in a fluid simulating the mixed cerebral-interstitial fluid of the neurovascular unit. [17] For these studies, we have also chosen to use as a supplement Fetal Bovine Serum (FBS) which is routinely used in cell cultures, and as model proteins transferrin (TrF), albumin (Alb) and ferritin (FrT). It has to be noted that the concentrations that were chosen for each protein were modified based on the literature, and correspond to the amounts that can be found both in the cell culture media and in the cerebrospinal fluid.[18]

The results that are presented in **Fig. 2** demonstrate different behaviors depending on the combination of NCubes/CM-NCubes and proteins that are tested. When FBS or Alb are used, NCubes and CM-NCubes demonstrate excellent colloidal stability as it can be seen in **Fig. 2A-1** and **2A-3** and in **Fig. 2B-1** and **2B-3** for NCubes and CM-NCubes, respectively. When other

proteins like transferrin and ferritin are used, we see that the nanoparticles start to aggregate resulting in multimodal populations (**Fig. 2A-2** and **2A-4** for NCubes using TrF and FrT, respectively, and **Fig. 2B-2** and 2**B-4** for CM-NCubes using TrF and FrT, respectively), with increased hydrodynamic diameters and high polydispersity. Since albumin is the main component of FBS and since both albumin and FBS data show similar behavior, we assumed that albumin is the protein that interacts with the fabricated NCubes and CM-NCubes and increases their stability inside the aCSF. In order to further strengthen our assumption, we assessed the behavior of NCubes and CM-NCubes in aCSF containing albumin, transferrin, and ferritin, and we have seen that the polydispersity and the hydrodynamic diameter is decreased for both NCubes and CM-NCubes, having the best results in terms of stability for the cell membrane-coated particles. These results not only suggest that the colloidal stability of the nanoparticles is affected mostly from albumin, but also that the cell membrane-coated particles differently interact compared to the uncoated ones. This behavior can be attributed to the fact that the NCubes have a high surface area (34 $m^2 g^{-1}$) and nanopores in the range of 2 nm (**Fig. S5-A** and **Fig. S5-B** ESI†), that allows more proteins to be physically adsorbed on their surface resulting into the creation of a thick protein corona layer composed by all the supplemented proteins, and that leads to the distributions observed in **Fig. 2A-5**.

In order to further evaluate the colloidal stability of the particles, we performed dynamic light scattering studies at different time points (0, 1, 6 and 24 h) in distilled water, DMEM and DMEM + 10% FBS (**Fig. S6**, ESI†). The results demonstrated that both coated and uncoated samples are stable up to 6 h when they are dispersed in distilled H_2O or DMEM + 10% FBS. At all the time points up to 6 h, CM-NCubes present a lower average hydrodynamic diameter (120.0 ± 2.8 nm in H_2O and 165.0 ± 6.1 nm in DMEM + 10 % FBS) compared to the

uncoated NCubes (198.0 ± 23.3 nm in H_2O and 264.0 ± 4.5 nm in DMEM + 10 % FBS) and this may be attributed to an increased stability because of the coating. The higher colloidal stability that is presented in distilled water compared to the other two used media may also be attributed to the negative surface charge of -17.2 ± 0.2 mV for the NCubes and of -20.9 ± 0.4 mV for the CM-NCubes. Due to the high ionic strength of DMEM, the results for the NCubes and CM-NCubes are similar, suggesting the creation of aggregates. The results are more evident after 24 h, when the NCubes present a value of 1.2 ± 0.1 μm and 250.0 ± 6.2 nm for H_2O and DMEM + 10% FBS respectively (**Fig. S6A-4**, ESI†), in contrast to the coated ones (**Fig. S6B-4**, ESI†), where the average hydrodynamic diameter is 272.0 ± 5.1 and 160.0 ± 3.0 nm for H_2O and DMEM + 10% FBS, respectively.

In order to assess how the oxidative microenvironment of the tumor may affect the stability of the CM-NCubes, we performed again dynamic light scattering studies incubating the particles with increasing concentrations of H_2O_2 (0.05, 0.25 and 1 mM) diluted in aCSF, which is a biologically relevant medium, containing albumin as a protein stabilizer, in order to simulate the various conditions of oxidative stress in glioblastoma. Although the concentration of H_2O_2 1 mM is quite high, we used it as a positive control in order to be sure that the cell membrane will be affected. These preliminary results (**Fig. S7**, ESI†) demonstrated that even at a concentration of H_2O_2 0.05 mM, after 72 h, the stability of the CM-NCubes can be affected, probably due to the lipid peroxidation of the cell membrane that can subsequently lead to partial membrane degradation. Similar behavior could also be observed as well at higher H_2O_2 concentrations.

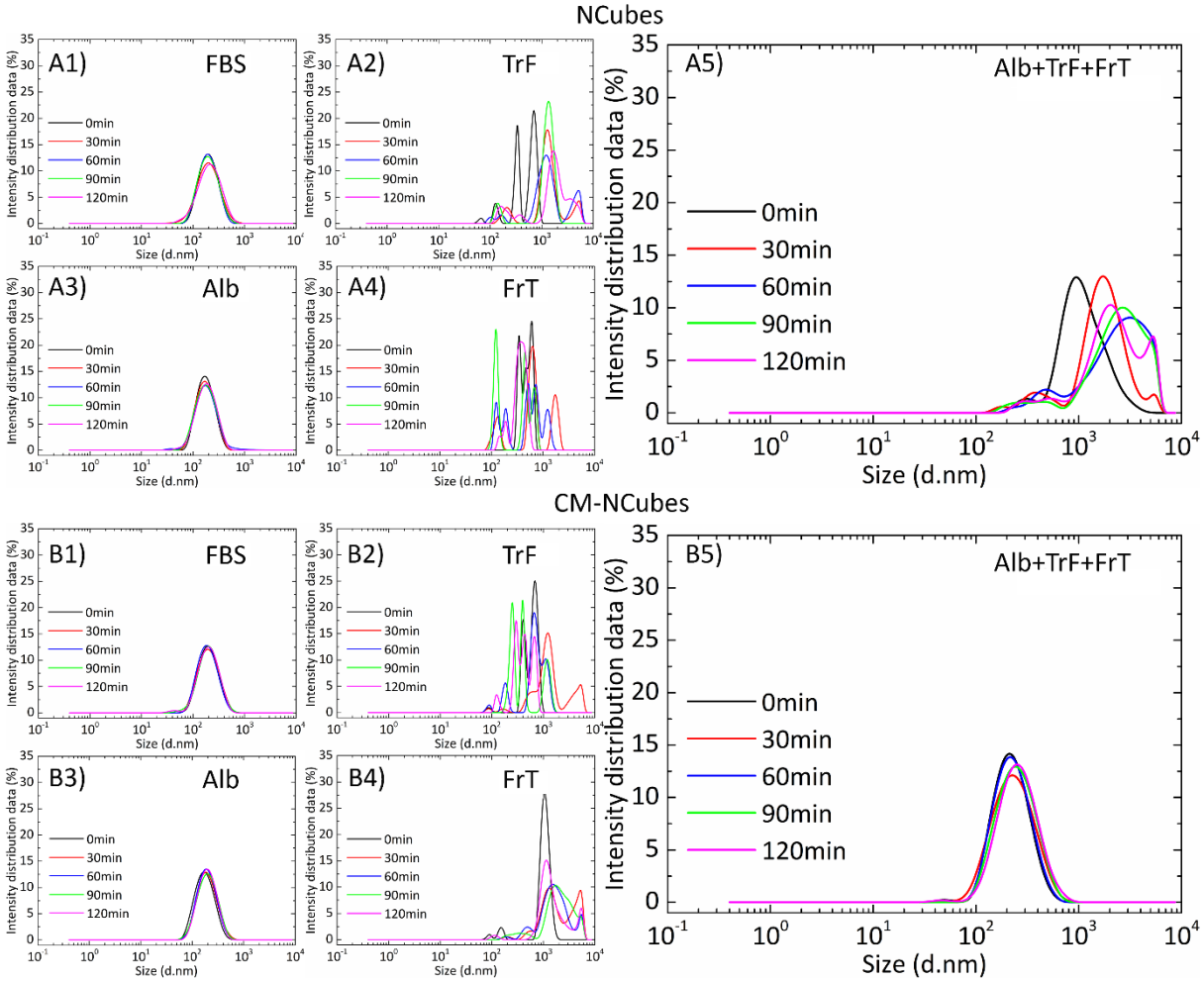

Figure 2. Dynamic light scattering studies presenting the hydrodynamic diameter of NCubes and CM-NCubes, after their interaction with different proteins (or their combination) found both in aCSF and in the blood plasma. A1) NCubes in aCSF + 10% FBS, A2) NCubes in aCSF + transferrin 200 μg ml^{-1}, A3) NCubes in aCSF + albumin 2.3 mg ml^{-1}, A4) NCubes in aCSF + Ferritin 1.5 ng ml^{-1}, and A5) NCubes + albumin 2.3 mg ml^{-1} + transferrin 200 μg ml^{-1} + ferritin 1.5 ng ml^{-1}; B1) CM-NCubes in aCSF + 10% FBS, B2) CM-NCubes in aCSF + transferrin 200 μg ml^{-1}, B3) CM-NCubes in aCSF + albumin 2.3 mg ml^{-1}, B4) CM-NCubes in aCSF + ferritin 1.5 ng ml^{-1} and B5) NCubes + albumin 2.3 mg ml^{-1} + transferrin 200 μg ml^{-1} + ferritin 1.5 ng ml^{-1}. All the measurements were performed in artificial cerebrospinal fluid at 37°C using a concentration of 100 μg ml^{-1} for both NCubes and CM-NCubes. The presented results derive from the average values of three different measurements at each time point.

2.3 Magnetic characterization and magnetic hyperthermia studies

In order for a hyperthermia-inducing agent to be successful, properties like high saturation magnetization, high specific absorption rate (SAR) and high intrinsic loss power (ILP) are needed. Aiming at assessing these properties, a series of magnetic characterization and response to external alternating magnetic fields have been carried out.

The magnetic properties of NCubes and CM-NCubes are presented in **Fig. 3A**, and show that the saturation magnetization is approximately 57 emu g^{-1} for the uncoated NCubes and 40 emu g^{-1} for the CM-NCubes, while the coercivity is approximately 12 mT for both NCubes and CM-NCubes. These values are close to those of nanoparticles reported in other studies,[19] and they show the potential ability of the CM-NCubes to be used as therapeutics for cancer.

After assessing the magnetic properties, we evaluated the ability of NCubes and CM-NCubes to increase the temperature of the surrounding medium under the influence of an alternating magnetic field, in three different media. From the graph presented in **Fig. 3B**, where 5 mg ml^{-1} of NCubes or CM-NCubes are exposed to a magnetic field of 20 mT with a frequency of 750 KHz, it can be observed that CM-NCubes behave better in terms of heating rate with respect to the uncoated ones. More specifically, CM-NCubes in water have the ability to increase the temperature from 32.5°C to 60.0°C in 60 min, while the corresponding uncoated ones reach 40°C in the same timeframe. Similar behavior can be observed when other media (DMEM and DMEM + 10% FBS) are used. This behavior can be probably attributed to the faster precipitation of the uncoated NCubes in media with high ionic strength (DMEM and DMEM + 10% FBS), leading to their accumulation at the bottom of the vial and outside the area where the magnetic field presents its maximum intensity. On the other hand, although the ability of the CM-NCubes to increase temperature is also affected by the used medium, still a higher temperature can be achieved after 60 min with respect to

the NCubes, and this can be attributed to the increased colloidal stability that they present, probably due to the phospholipid cell membrane coating. This stability allows the CM-NCubes to be homogeneously dispersed for longer periods, thus taking advantage of the maximum intensity of the magnetic field. Plain media (H_2O, DMEM and DMEM + 10% FBS) without coated or uncoated nanocubes were used as controls and the results are also presented in **Fig. 3B**. In order to assess the ability of the CM-NCubes to be used as a hyperthermia-inducing agent, we have calculated the SAR and the ILP values under various magnetic field intensities, various frequencies, and in various media. The results presented in **Fig. 3C** and **Fig. 3E** demonstrate that we can precisely control properties like SAR and ILP by controlling the magnetic field and the frequency, suggesting the precise control of the heating rate and the maximum temperature that can be achieved using a desired CM-NCubes concentration. It has to be noted that the best results were acquired when an AMF of 20 mT at 750 KHz and a 9 turn-44 mm coil were used, and for these parameters the highest obtained SAR and ILP values were 78.6 ± 3.9 W g^{-1} and 0.40 ± 0.02 $nHm^2 kg^{-1}$, respectively, values that are higher with respect to commercial Fe_3O_4 nanoparticles reported in the literature. [20] It has to be mentioned that high values of SAR (49.6 ± 2.4 W g^{-1}) and ILP (0.80 ± 0.04 $nHm^2 kg^{-1}$) were also obtained using a 56 mm coil and 12 mT at 657 KHz of AMF, values close to the Brezovich limit (4.85×108 A m^{-1} s^{-1}). [21] Nevertheless, for the *in vitro* evaluation of the CM-NCubes we have decided to use the maximum possible magnetic field and frequency, in order to overcome the limited heating efficiency. [19, 22] After assessing the effect of various magnetic field intensities and different coils, we evaluated the effect of the solvent on SAR and ILP values of NCubes and CM-NCubes (**Fig. 3D** and **Fig. 3F**). As expected from the results in Fig. 2B, the highest SAR and ILP values were obtained for CM-NCubes in water (78.6 ± 3.9 W g^{-1} and 0.40 ± 0.02 $nHm^2 kg^{-1}$), followed by the same particles

in DMEM + 10% FBS (63.0 ± 3.2 W kg^{-1} and 0.33 ± 0.02 nHm^2 kg^{-1}), and then in plain DMEM (53.8 ± 2.7 W g^{-1} and 0.28 ± 0.01 nHm^2 kg^{-1}). These results along with the temperature increment that is presented in Fig. 2B suggest that the ionic strength of the solvent and/or the supplements (*e.g.*, fetal bovine serum) in the medium have an effect on the SAR and ILP values, since they directly affect the colloidal stability of both NCubes and CM-NCubes (Fig. S6).

Overall, the results demonstrated that the CM-NCubes can act as hyperthermia-inducing agents not only in water but also in simulated body fluid media. Since magnetite nanoparticles have been robustly reported as good magnetic resonance imaging (MRI) contrast agents, [5, 23] we performed NMR relaxometry studies in order to evaluate the ability of the CM-NCubes to act as well as diagnostic tools. The results presented in the supporting information (**Table S5** and **Fig. S8**, ESI†) demonstrated that the CM-NCubes can be potentially used as T_2 MRI contrast agents, since they present relaxivity values r_2 = 174.60, 184.80, and 182.13 $s^{-1}mM^{-1}$ at frequencies of 56.7, 21.3 and 8.5 MHz respectively, that cover most of the typical fields, H = 1.33 T (near H=1.5 T), 0.5 T and 0.2 T respectively, of MRI tomographs used both in clinics and in research laboratories. It has to be noted that the commercial T_2 MRI contrast agent Endorem® shows $r_2 \cong 100$ $s^{-1}mM^{-1}$ (in the range 8.5 MHz < v < 60 MHz).[13] In addition to NMR relaxometry studies, phantom images of CM-NCubes dispersions, water, and of the commercial contrast agent Endorem®, for a high resolution Spin Echo sequence, are presented in **Fig. S8-B**. It is clear that the CM-NCubes signal is darker (41.6% ± 1.4% signal intensity compared to the water signal which was considered as 100%) than Endorem® (45.7% ± 2.5% signal intensity compared to the water signal) at a similar concentration (0.08 mM for CM-NCubes and 0.1 mM for Endorem®) of the magnetic

component, and therefore shows a better performance as a negative contrast agent at the imager operating frequency (8.5 MHz).

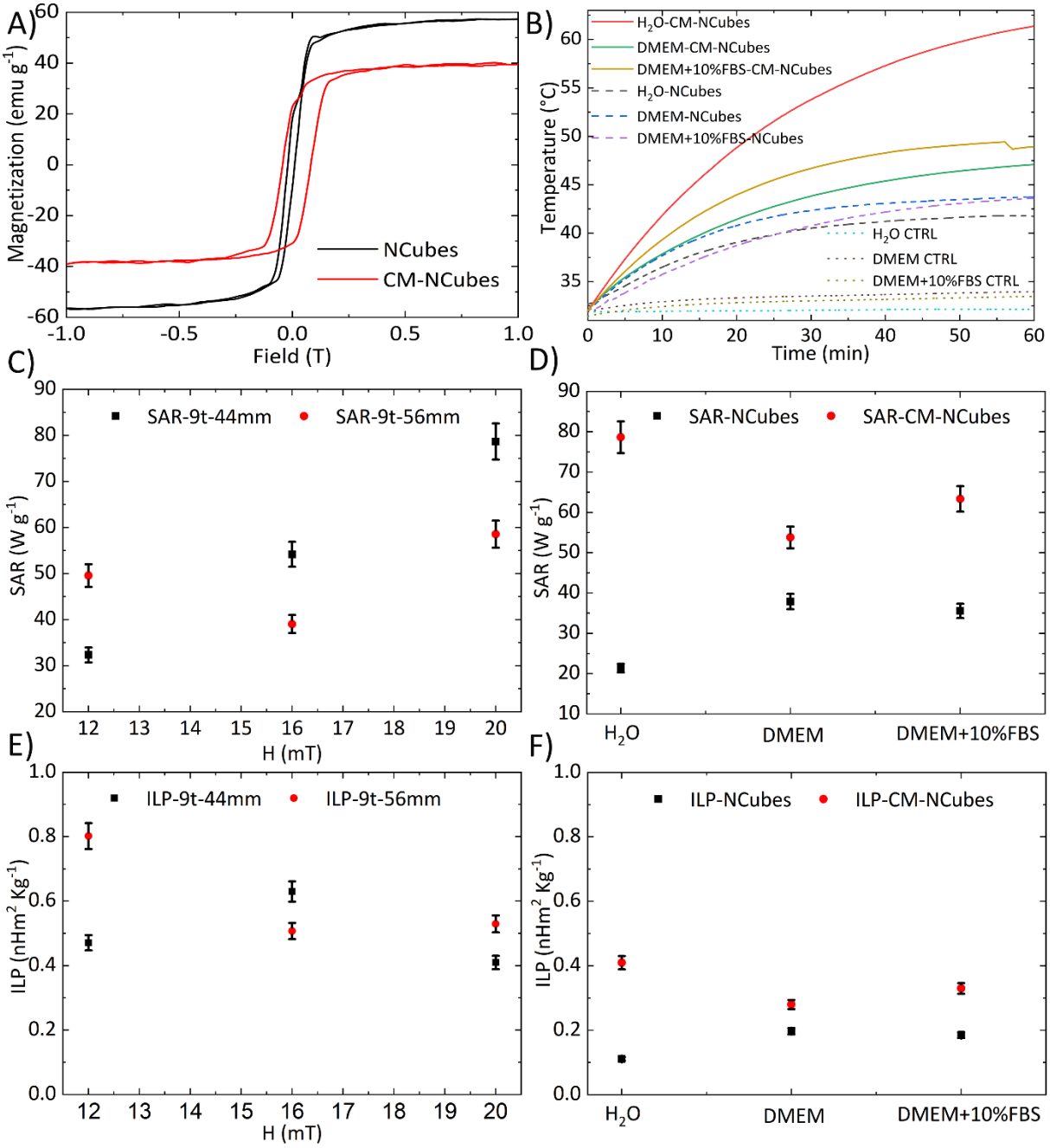

Figure 3. A) Hysteresis loops of NCubes (black curve – M_s = 57 emu g^{-1}) and CM-NCubes (red curve – M_s = 40 emu g^{-1}) normalized to the inorganic component; B) temperature increment over time, after the exposure of plain media, NCubes, and CM-NCubes dispersed in different media to an AMF of 20 mT – 750 KHz obtained with a 9 turn-44 mm coil; C) SAR values of CM-NCubes after their exposure at various intensities of AMFs using 2 different diameter coils; D) SAR values of NCubes and CM-NCubes in various media; E) ILP values of CM-

NCubes after their exposure at various intensities of AMFs using 2 different diameter coils; D) ILP values of NCubes and CM-NCubes in various media (*n* = 3).

2.4 Oxygen generation and temperature increase due to ROS scavenging

It is well-known that solid tumors share some common characteristics, like the overproduction of ROS and the hypoxic microenvironment.[8a, 8b]Moreover, hypoxia has been related to increased angiogenesis and metastatic spreading of cancer cells, as well with the multidrug resistance phenomenon.[8b-d] Taking this into consideration, we hypothesized that the MnO_2 component of the CM-NCubes could scavenge the overproduced ROS, while at the same time will increase the oxygen levels due to the reaction of MnO_2 with hydrogen peroxide.[6a, 6b, 6e] In addition, we hypothesized that since the scavenging reaction is an exothermic reaction, it will locally increase the temperature inside cells. In order to evaluate the increment of oxygen levels, we have tested five different concentrations of H_2O_2 (0, 0.05, 0.25, 0.5 and 1 mM), interacting with three different concentrations of CM-NCubes. The results presented in **Fig. 4A** demonstrate that the amount of the oxygen produced is related both to the concentration of the CM-NCubes as well as to the concentration of the H_2O_2, as already shown in our previous study.[6b] Furthermore, it is noteworthy the fact that even at the lowest concentration of CM-NCubes (100 μg ml^{-1}, **Fig. 4A-1**), where according to the ICP results the Fe/Mn ratio is 10.5 (meaning that the percentage of manganese is 10.5 times lower than iron, *e.g.*, $MnO_2 \approx 8.4$ μg ml^{-1}), an increment of oxygen concentration in the range 1-10% could be observed depending on the H_2O_2concentration used, suggesting a controlled generation of oxygen even at low concentrations of CM-NCubes. Similar results were also obtained when higher concentrations of CM-NCubes were used (**Fig. 4A-2** and **Fig. 4A-3**), suggesting that the highest used concentration of H_2O_2 (1 mM) can be completely scavenged by using 100 μg ml^{-1} of CM-NCubes. In order to verify the scavenging ability of the fabricated

CM-NCubes, we used a total antioxidant capacity assay kit, and we compared the antioxidant ability of the CM-NCubes with the antioxidant ability of Trolox, which is a standard analog of vitamin E. The results presented in **Fig. S9** (ESI†) show, similarly to the oxygen generation results, that the antioxidant ability is dose-dependent, with 100, 250 and 500 μg ml^{-1} of CM-NCubes to be analogue, in terms of antioxidant activity, to 17.5 ± 1.13 μM, 50.3 ± 3.2 μM and 103.3 ± 6.7 μM of Trolox, respectively.

As previously mentioned, the reaction between H_2O_2 and MnO_2 is exothermic, and can possibly locally increase the temperature. In order to assess this ability, we measured the increment of temperature after the reaction between CM-NCubes and H_2O_2 at the same concentrations used for the oxygen generation measurements. The results presented in **Fig. 4B** show an increment of temperature up to 0.75°C (**Fig. 4B-1** and **Fig. 4B-2**) when the highest concentration of H_2O_2 (1 mM) is used, while a temperature increase around 0.25°C can be observed for lower concentrations of H_2O_2. Although we would have expected similar results when the highest amount (500 μg) of CM-NCubes was used, it can be seen (**Fig. 4B-3**) that the highest increment is between 0.25 and 0.35°C, and this may be attributed to the fact that magnetite constitutes a material with increased heat capacity and thermal conductivity [24], that can absorb the generated heat produced by the exothermic reaction, thus showing, on the whole, a reduced temperature increment. Moreover, since our system is not thermodynamically closed? Check I am not sure, thermal exchanges of the medium with surrounding environment may contribute to the temperature differences in relation to the concentration of the CM-NCubes (Fig. 4B-1, 4B-2, 4B-3). Since the ability of CM-NCubes to increase temperature was proved by simply allowing the reaction between MnO_2 and H_2O_2, we evaluated the ability of the system to increase the intracellular temperature. In order to achieve this, we treated U-251 MG cells with CM-NCubes (250 μg ml^{-1}) overnight,

and subsequently, we stained the cells with a temperature sensitive dye as previously described.[25] Then, by using confocal microscopy, we recorded the difference in terms of fluorescence intensity in cells incubated with CM-NCubes, after the addition of DMEM supplemented with 25 mM of (4-(2-hydroxyethyl)-1-piperazine ethane sulfonic acid) (HEPES) (**Fig. 4C**, Control, and **Video S1**, ESI†) and after the addition of 100 μM of H_2O_2 in DMEM supplemented with HEPES (**Fig. 4C**, Treated, and **Video S2**, ESI†). In addition, in order to check the effect of the plain H_2O_2, we also performed studies using a second control, which we considered as a negative control (N. Control), where 100 μM of H_2O_2 in DMEM supplemented with HEPES was added to non-treated U-251 MG cells (**Fig. 4C**, N. Control, and **Video S3**, ESI†). It is evident from the reported representative images that until 80 s both of the samples demonstrate a stable fluorescence intensity, which remains stable when DMEM supplemented with HEPES is added, while after the addition of H_2O_2 the fluorescence intensity is significantly reduced. The reduction in the fluorescence intensity was translated in terms of temperature increment (**Fig. 4D**), and it was found that the intracellular temperature increased by 6°C in the samples treated with 100 μM H_2O_2, in contrast to the control cultures that were treated just with DMEM supplemented with HEPES, where no changes of temperature were recorded. We would like to stress out the fact that this is the first time that a drug delivery system like the presented one is shown to increase the intracellular temperature due to a simple ROS scavenging effect. These data suggest that it is possible to develop ROS-responsive systems presenting the ability to induce hyperthermia by simply scavenging the overproduced ROS in the cancerous microenvironment.

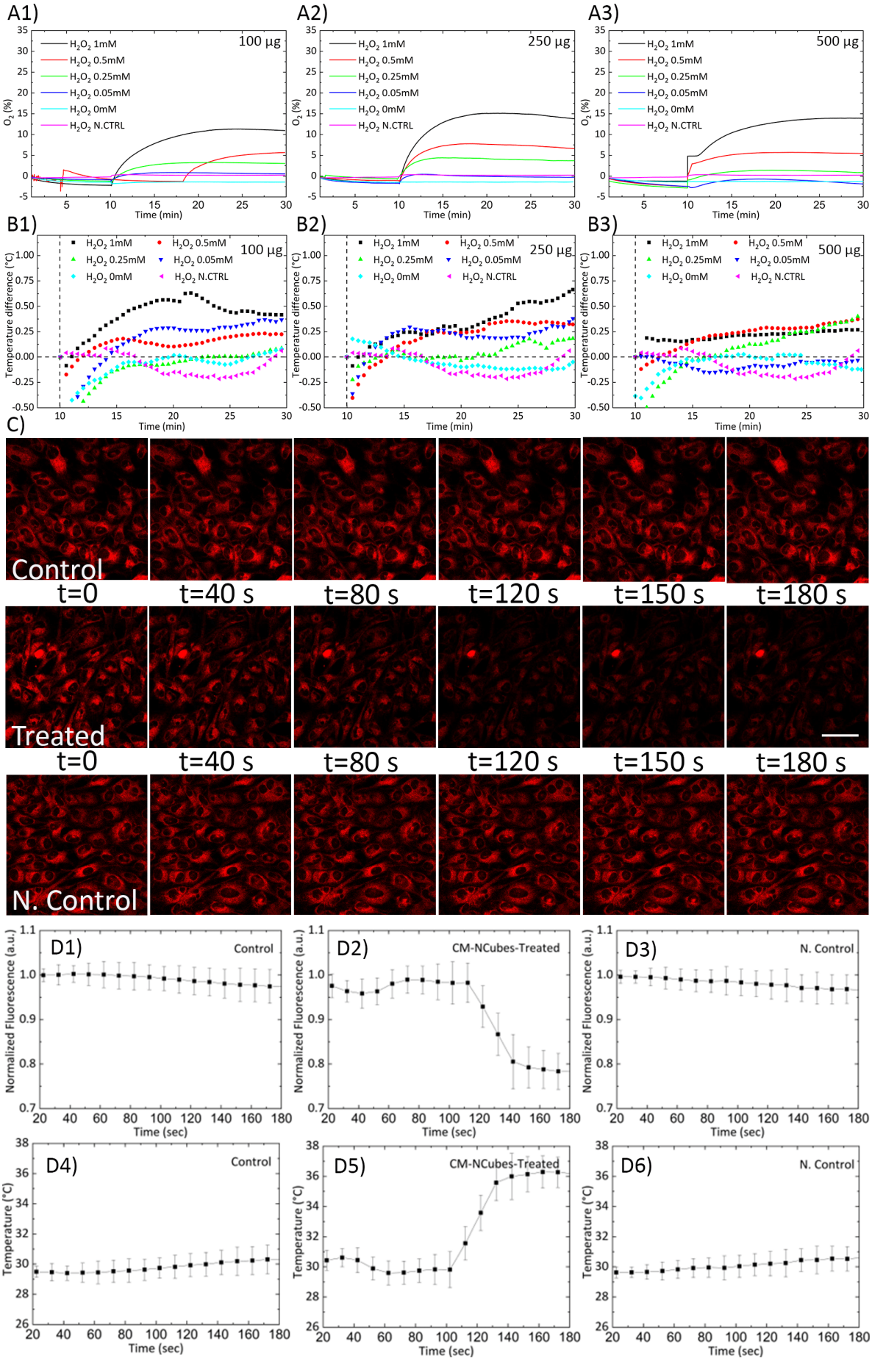
A1)
A2)
A3)
100 µg
250 µg
500 µg
H2O2 1mM
H2O2 0.5mM
H2O2 0.25mM
H2O2 0.05mM
H2O2 0mM
H2O2 N.CTRL
O2 (%)
Time (min)
B1)
B2)
B3)
Temperature difference (°C)
C)
Control
Treated
N. Control
t=0
t=40 s
t=80 s
t=120 s
t=150 s
t=180 s
D1)
D2)
D3)
D4)
D5)
D6)
CM-NCubes-Treated
Normalized Fluorescence (a.u.)
Temperature (°C)
Time (sec)

Figure 2. A) Oxygen generation and B) temperature increment after the reaction of different concentrations of CM-NCubes (100, 250 and 500 μg ml^{-1}) with increasing concentrations of H_2O_2 (0, 0.05, 0.25, 0.5 and 1 mM). H_2O_2 1 mM reacting with plain medium (H_2O_2 N. Control) was used as a negative control both in the oxygen generation and in the temperature measurements; C) confocal images showing the difference of fluorescence intensity in U-251 MG cells incubated with 250 μg ml^{-1} of CM-NCubes overnight after the addition of plain DMEM supplemented with 25 mM HEPES (control), and after the addition of 100 μM of H_2O_2 (at 80 s) (treated); D1) fluorescence intensity of the temperature sensitive dye in the control samples (addition of plain DMEM supplemented with HEPES in U-251 MG cultures incubated with 250 μg ml^{-1} of CM-NCubes overnight), D2) fluorescence intensity of the temperature sensitive dye after the addition of 100 μM of H_2O_2 in U-251 MG cultures incubated with 250 μg ml^{-1} of CM-NCubes overnight, D3) fluorescence intensity of the temperature sensitive dye after the addition of 100 μM of H_2O_2 in non-treated U-251 MG cultures (N. Control), D4) intracellular temperature of the control sample which remains stable at approximately 30°C; D5) intracellular temperature increment up to approximately 33°C after the addition of 100 μM of H_2O_2 in U-251 MG cultures incubated with 250 μg ml^{-1} of CM-NCubes overnight, D6) intracellular temperature of the negative control sample which remains stable after the addition of 100 μM of H_2O_2 in non-treated U-251 MG cultures

2.5 Loading and release studies

The ability of the CM-NCubes to be loaded with a chemotherapeutic drug and their ability to release this drug in a controlled manner was assessed through loading and release studies. Loading assessment showed that CM-NCubes can have an encapsulation efficiency (%EE) of 94.6± 4.6%, and dynamic loading (%DL) of 8.6 ± 1.2%.

The release studies (**Fig. S10**, ESI†), were performed at two different pH values (7.4 and 4.5), that respectively correspond to physiological pH and pH that can be found in the intracellular acidic organelles like lysosomes, as well as under the influence or not of an alternating magnetic field. The results demonstrate a slow and sustained release of SOR for a period of 192 h, even when two different stimuli like AMF and pH are applied.

After 6h, the release at pH 7.4 without and with AMF is respectively 5.5 ± 0.6% and 10.4 ± 2.6%, while at pH 4.5 without AMF and with AMF it is respectively 10.6% ± 2.1% and 11.3 ± 5.0%. Although there is a difference between pH 7.4 and pH 4.5 with and without the presence of the AMF, this difference is not significant and may be attributed to a burst release occurring during the first hours. Nevertheless, the released amount of sorafenib at this time point is very low, and cannot be considered significant. After 192 h the cumulative release at pH 7.4 reaches 23.0% ± 0.9%, at pH 7.4 + AMF reaches 28.3% ± 2.4%, at pH 4.5 reaches 45.0% ± 1.9% and finally at pH 4.5 + AMF reaches 51.9% ± 1.9%. These results demonstrate that there is a controlled and sustained release over a period of 192 h which can be modulated by combining different temperatures and pH values.

2.6 Targeting ability – Internalization studies

In order to assess the ability of CM-NCubes to be specifically internalized by the homotypic U-251 MG cell line, we carried out experiments using four different cell lines, as well as NCubes covered by a biocompatible lipid-based coating as a control. The chosen cell lines were, besides U-251 MG, C8-D1A (astrocytes) and bEnd.3 (endothelial cells) as the main cell lines that constitute the BBB model, and SH-SY5Y as a different type of brain cancer cells. Furthermore, we also assessed the internalization of NCubes functionalized with a lipid-based coating (LP-NCubes) made of biocompatible lipids (*e.g.*, cetyl palmitate, glycerol monooleate, and 1,2–distearoyl–sn–glycerol–3–phosphoethanolamine–N–[methoxy(polyethylene glycol)]), already reported in the literature also by our group.[19, 26] The internalization was assessed by using both flow cytometry and confocal microscopy. The results presented in **Fig. 5A** and **5B** make evident that there is preferential uptake of CM-NCubes with respect to LP-NCubes for all the cell lines, with the exception of the bEnd.3,

that apparently after 4 h shows a higher internalization of LP-NCubes compared to the CM-NCubes. Despite this qualitative evidence, the statistical analysis (one-way ANOVA, **Table S6**, ESI†) show that this difference is not significant. Furthermore, a non-significant difference was also observed between LP- and CM-NCubes tested on C8-D1A and SH-SY5Y cells, while the difference was significant between LP- and CM-NCubes, in favor of CM-NCubes, in U-251 MG cells ($p < 0.01$). These results suggest that CM-NCubes show a preferential uptake by the homologous cancerous cell line with respect to the SH-SY5Y, C8-D1A and bEnd.3 cells. Furthermore, there is a significant difference, with a preferential uptake, in the CM-NCubes internalization by the homotypic U-251 MG cell line ($p <0.0001$) with respect to the SH-SY5Y and C8-D1A, respectively.

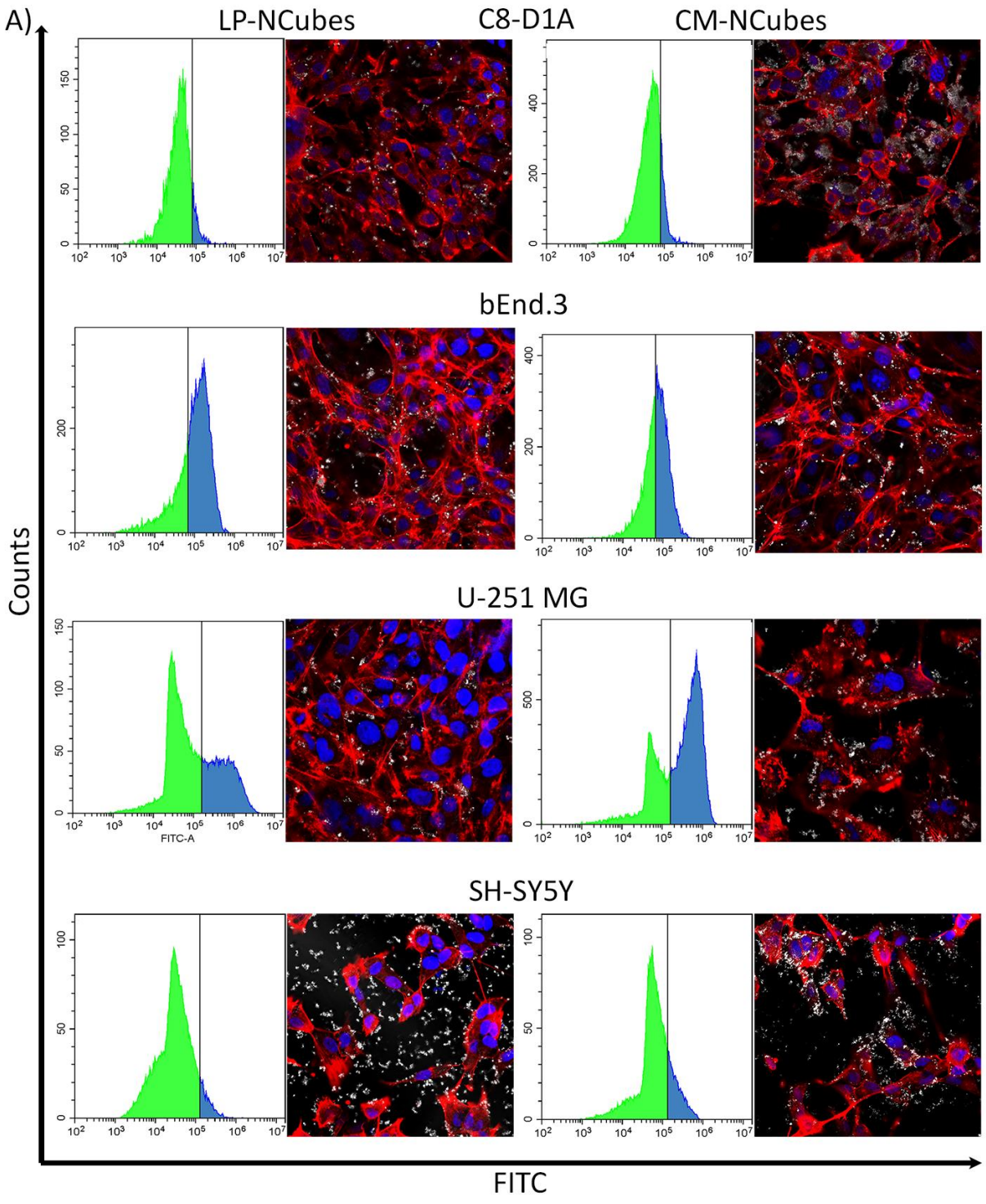
A)
LP-NCubes
C8-D1A
CM-NCubes
bEnd.3
U-251 MG
SH-SY5Y
Counts
FITC
FITC-A

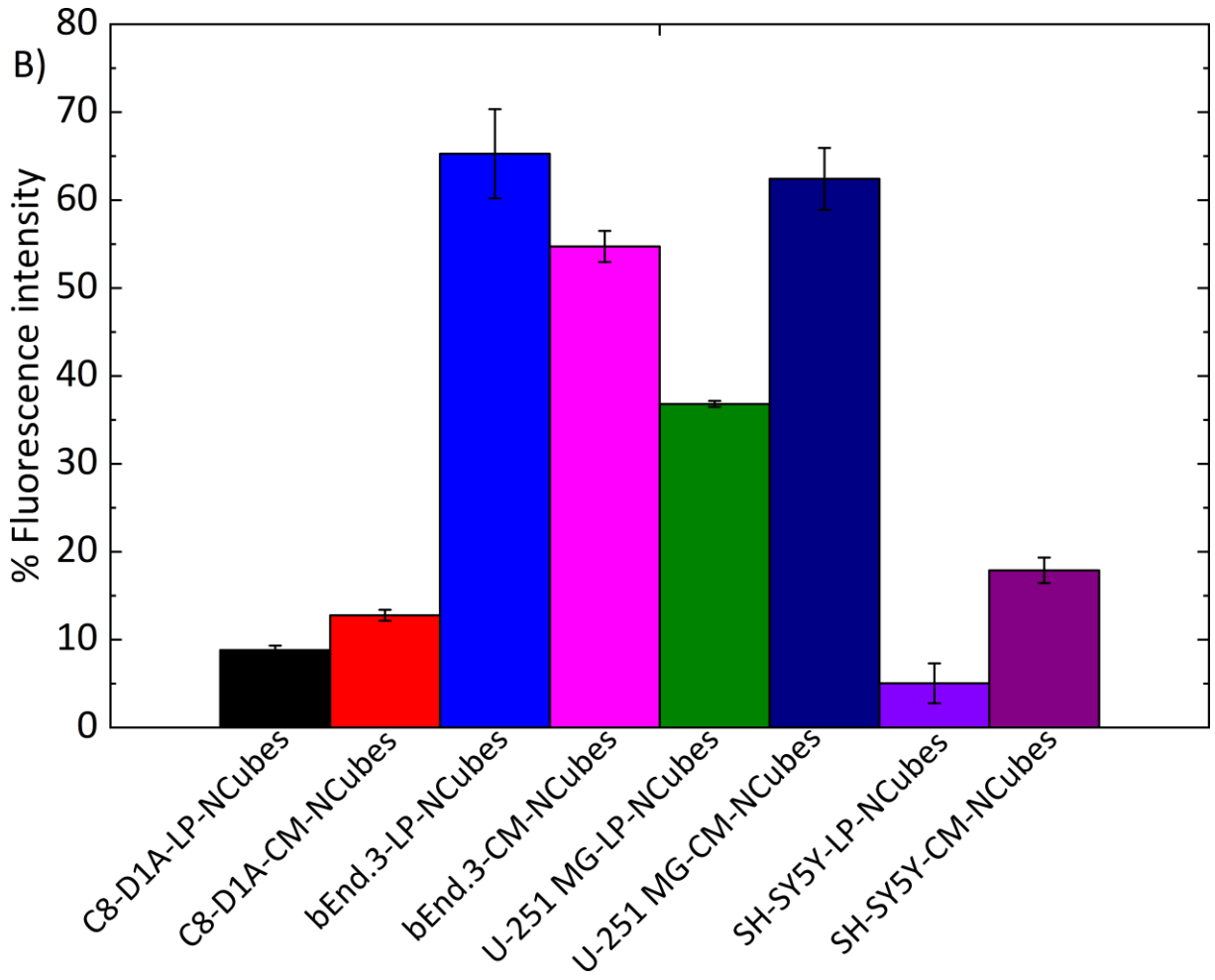

Figure 3. **A)** Flow cytometry graphs and corresponding confocal images of internalized CM-NCubes and LP-NCubes, after 4 h, by C8-D1A, bEnd.3, U-251 MG and SH-SY5Y cells. For the flow cytometry analysis, all the cell lines were treated with DiO-stained CM-NCubes and LP-NCubes (in the histograms with the green color are depicted the fluorescence negative cells (-) and in blue the fluorescence positive cells (+)); for the confocal images the particles were unstained (nuclei in blue; f-actin in red; CM-NCubes in white); **B)** bar plots summarizing the cells' fluorescent intensities as they were calculated from the flow cytometry analysis. (*n* =3, one-way ANOVA, a detailed statistical analysis is provided at Table S6, ESI†).

2.7 Blood-brain barrier crossing

One of the biggest challenges for the treatment of glioblastoma, as well as of other central nervous system diseases, is the crossing of the BBB and the successful delivery of the pharmaceutical cargo in the pathological tissue. Aiming at assessing the ability of CM-

NCubes to cross the BBB, we used an *in vitro* cell culture model, previously described in another work of our group.[19] The results presented in **Fig. 6A** show a sustained passage of CM-NCubes that were incubated onto a monolayer of bEnd.3 cells, seeded on a 3 µm pore Transwell© insert, and that after 48 h, 75.0 ± 3.7% of the incubated CM-NCubes (calculated according to a standard curve of DiO-stained CM-NCubes previously performed), were able to pass the endothelial layer. These data show the potential of the fabricated system to be used as a biomimetic drug delivery system for the passage of the BBB. After BBB in vitro model crossing, CM-NCubes were efficiently internalized by U-251 MG cells, as demonstrated by confocal microscope observation (**Fig. 6B**, single acquisition, and **Fig. 6C,** Z-stack rendering).

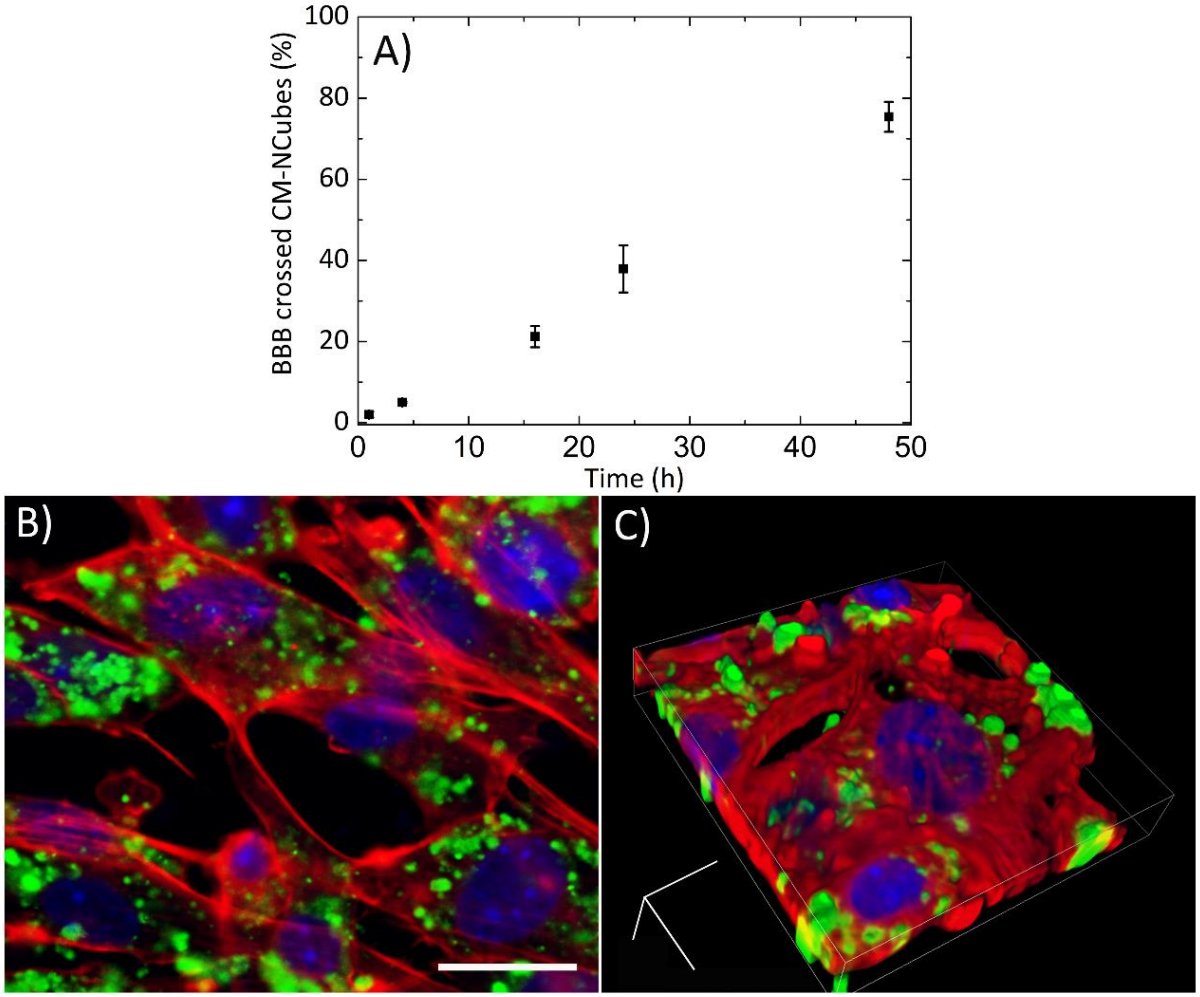

Figure 6. A) Percentage of DiO-stained CM-NCubes crossing a bEnd.3 monolayer resembling an *in vitro* BBB model, with respect to the initial CM-NCubes seeded in the abluminal part of the Transwell© insert; **B)** 2D and **C)** 3D confocal acquisitions showing CM-NCubes internalized by U-251 MG cells after BBB crossing (nuclei in blue; f-actin in red; CM-NCubes in green). Scale bar for B: 25µm, For C: x: 0.10 µm, y: 0.10 µm, z: 0.13 µm; width: 53.25 µm, height: 53.25 µm, depth: 8.88 µm. *n* = 3, one-way ANOVA, $p<0.5$

2.8 Magnetic targeting using an in vitro dynamic model of the BBB

The ability of CM-NCubes to be attracted and accumulated into a specific area of interest in a microfluidic BBB *in vitro* model was assessed using a static magnetic field generated by a magnet. We further studied this accumulation by using a theoretical numerical model that was previously described by our group. [14]

The observed CM-NCubes distribution after exposure to a static magnetic field as shown in **Fig. 7A** (fluorescence intensity coded with pseudocolors) and **Fig. 7B** was successfully predicted by the numerical model that is presented in **Fig. 7C**. By accounting for viscous effects (fostering accumulation closer to the channel boundaries), the model predicted a higher density of captured CM-NCubes near the magnet top edge, as well as a lower density spread on the magnet top surface. After accumulation, CM-NCubes were able to be internalized by both the bEnd.3 cells seeded in the upper channel of the fluidic device as well as U-251 MG cells present in the lower compartment of the system. Without the use of a static magnet, the amount of CM-NCubes internalized by both cell lines was significantly reduced, as shown in **Fig. 8**.

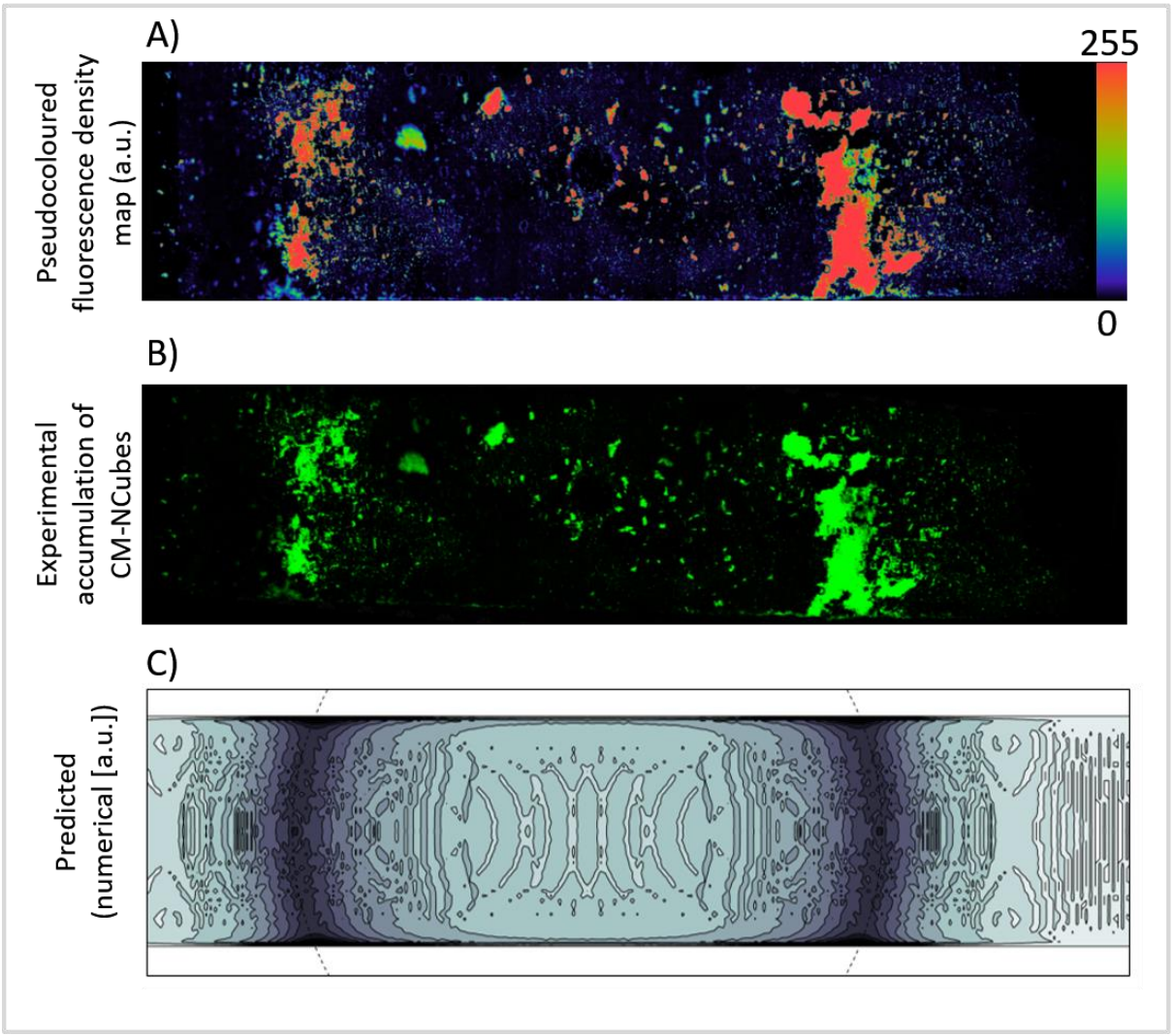

Figure 7. A) Pseudo colored fluorescence density distribution of the CM-NCubes after their exposure to a static magnetic field placed under the fluidic BBB channel; **B)** Distribution of DiO-stained (green) CM-NCubes overlapped with a dark field image of the fluidic channel; **C)** density contour plot (a.u.) of the captured CM-NCubes, as predicted by the numerical model (the dashed line denotes the top edge of the underlying magnet).

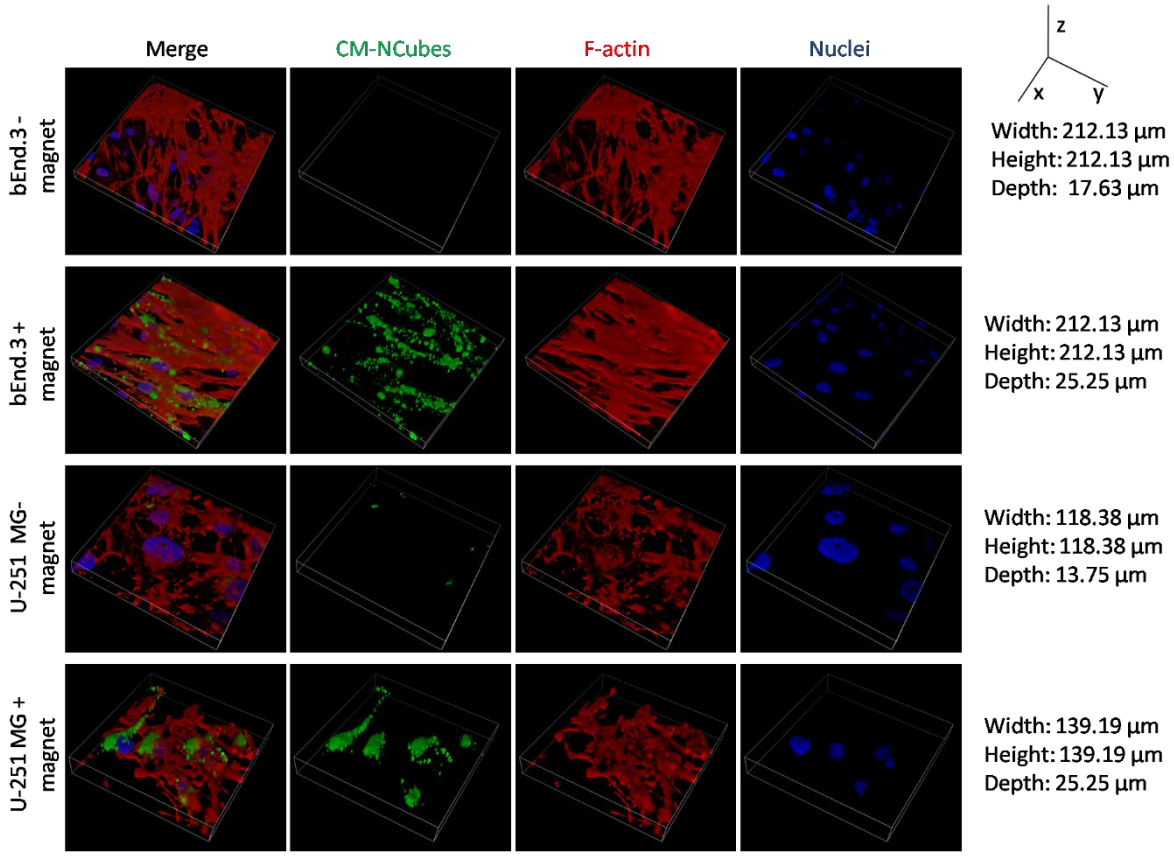

Figure 8. Internalization of DiO-stained CM-NCubes by both bEnd.3 cells and U-251 MG cells seeded in the fluidic BBB *in vitro* system with and without the presence of a static magnet (Nuclei in blue; F-actin in red; CM-NCubes in green).

2.9 Magnetic hyperthermia-induced apoptosis, increased caspase activation and reactive oxygen (ROS) and nitrogen (RNS) species generation

The ability of CM-NCubes and SOR-CM-NCubes to induce apoptosis was studied with or without the exposure of U-251 GM spheroids to an external alternating magnetic field. The results presented in **Fig.9A** show that the alternating magnetic field does not have an effect to the plain U-251 MG spheroids (live cell: 91.3% ± 0.6%, early apoptotic cells 0.4% ± 0.3%, late apoptotic cells 0.2% ± 0.1%,and dead cells 8.1% ± 0.2%). When the spheroids are treated with plain sorafenib (10 µg ml^{-1}), early and late apoptotic cells as well as dead cells increase to 1.8% ± 0.5%,1.1% ± 0.2% and 10.9 % ± 0.4% without exposure to the AMF, and to 1.5% ±

0.2%, 2.8% ± 0.9% and 13.5% ± 3.7% % after their exposure to the AMF, respectively. These results, in combination to the performed statistical analysis, demonstrate that there is no significant difference in the viability of the U-251 MG spheroids, between the control and the group treated with SOR, with or without the exposure to the AMF.

On the other hand, when the U-251 MG spheroids are treated with CM-NCubes, there is an increase in late apoptotic (9.7% ± 4.6%) and dead (24.3% ± 0.1%) cells when an AMF is used. This increase in the dead cells is considered significant ($p < 0.0001$) compared to the control group. The spheroids incubated with CM-NCubes that have not been exposed to an AMF present 80.2% ± 0.3% of live cells, 2.1% ± 0.6% of early apoptotic cells, 1.7% ± 0.3% of late apoptotic cells and 15.9% ± 0.3% of dead cells versus 64.0% ± 4.3%, 1.9% ± 0.2%, 9.7% ± 4.6%, and 24.3% ± 0.1%, respectively for the spheroids exposed to an AMF (**Fig. S11**, ESI†). These results demonstrate firstly that the CM-NCubes do not affect the viability of the spheroids since there is no significant difference between the control group and the group treated with CM-NCubes, unless if an AMF is applied. The group treated with CM-NCubes and exposed to the AMF reduces the percentage of live cells to 64.0% ± 4.3% ($p < 0.0001$ compared to the control). The effect of magnetic hyperthermia-induced apoptosis is more evident when sorafenib-loaded CM-NCubes are used. Without the use of an AMF, the percentage of live cells is 79.9% ± 4.9% and early apoptotic, late apoptotic and dead cells are 1.7% ± 0.1%, 1.4% ± 0.1%, and 17% ± 4.9%, respectively. The fact that SOR-CM-NCubes do not significantly increase the percentage of apoptotic and dead cells suggests that the encapsulated sorafenib is slowly released from the CM-NCubes if the AMF is not applied. Conversely, the percentage of live cells when the AMF is used decreases to 55.3% ± 4.5%, while the percentages of the early apoptotic, late apoptotic and dead cells changes to 2.8% ±

1.0%, 14.4% ± 0.1%, and 27.6% ± 3.3%, respectively. It is obvious that increased apoptosis and cell death can be observed when a combination of sorafenib and AMF is used.

Aiming at further investigating the apoptotic pathway during hyperthermia, we assessed the enzymatic activity of caspase 3 and caspase 9. The results presented in **Fig. 9B** and **Fig. 9C**, respectively, and the statistical analysis (**Table S7** and **Table S8**, ESI†) show that there is no significant difference in the activity of caspase 3 (cas-3) in the majority of the groups, with the exception of the SOR-CM-NCubes group after its exposure to the AMF where a significant difference ($p < 0.5$) is present (3.0 ± 0.2 fold increase), compared to the control group and to the group treated with the CM-NCubes but without AMF application (1.0 ± 0.5 N-fold increase). In addition, a significant difference ($p < 0.01$) is also observed between the group treated with sorafenib (0.6 ± 0.4 fold increase) and the SOR-CM-NCubes+AMF group (3.0 ± 0.2 fold increase). These results suggest that the cas-3 pathway is activated only when sorafenib and alternating magnetic field are combined, and this may be attributed to the small concentration of drug internalized by the cells when it is free, or because of its low release when the AMF is not applied (ca. 4.3 μM after 192h/pH 7.4 and 7.2 μM after 192h/pH 4.5). These results are in agreement with the work of Rodríguez-Hernández *et al.* [27], where it was presented that small concentrations of sorafenib (10 nM) do not result in cas-3 activation, but they can induce activation of the caspase 9 (cas-9) pathway, whereas higher concentrations (10 μM) can result in the activation of the cas-3 pathway as well. The increased levels of cas-3 can also be attributed to the alternating magnetic field since it has been already reported[28] that magnetic hyperthermia induces cas-3 activation. Continuing in **Fig. 9C**, it is more evident that cas-9 activation levels are higher compared to the cas-3 activation for the SOR-CM-NCubes groups, with and without an AMF, with the higher activity in the SOR-CM-NCubes+AMF group (7.5 ± 0.2 fold increase), which is significantly higher ($p <$

0.0001) with respect to the control group. Once more, a significant difference ($p < 0.001$) can be observed between the SOR group and the SOR-CM-NCubes+AMF group. A more detailed statistical analysis is provided in **Table S7** and **Table S8**, ESI†.

In order to assess whether the induced apoptosis is ROS/RNS-related, we also studied the increment of ROS and RNS level generation for each one of the tested conditions. The results presented in **Fig.9D** and **Fig.9E** respectively demonstrate that there is a significant increment in ROS generation in the CM-NCubes +AMF (5.5 ± 0.3 fold increase; $p < 0.0001$), and SOR-CM-NCubes +AMF (5.0 ± 0.1 fold increase; $p < 0.001$) treatments, compared to the control groups, which may be related with the increased percentages of apoptotic and dead cells that were described above. An increment can also be observed in the groups treated with free CM-NCubes (2.3 ± 0.1 fold increase) and in the group treated with SOR-CM-NCubes (3.6 ± 2.2 fold increase), but this difference is not considered significant. Although a significant ROS generation was observed during the AMF treatment, no significant increase could be observed in the reactive nitrogen species in the tested conditions, suggesting that the induced apoptosis may be attributed to ROS generation. A more detailed statistical analysis is provided in **Table S9** and **Table S10**, ESI†.

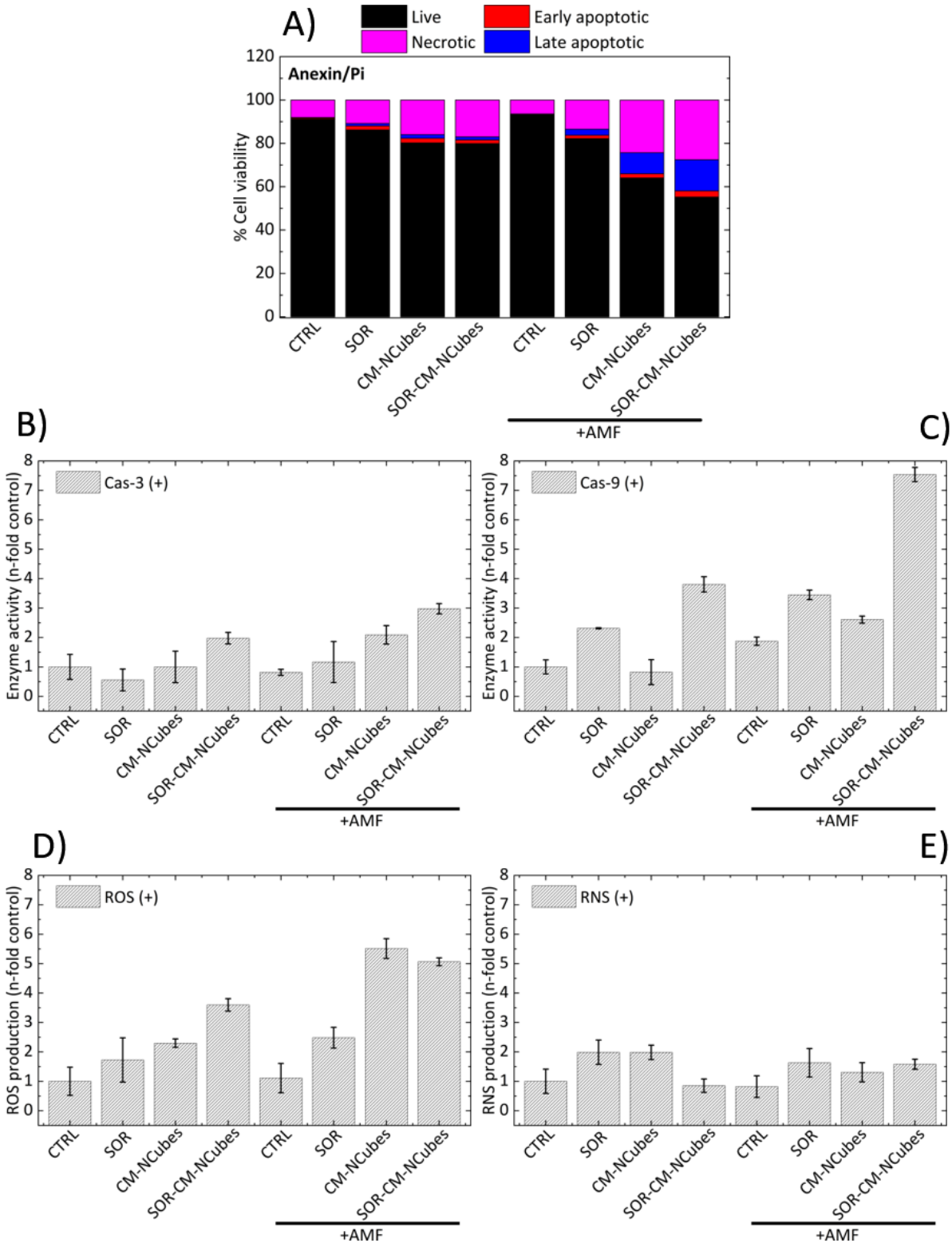

Figure 9.Bar graphs presenting **A)** the AMF-induced apoptosis, **B)** the n-fold increase in fluorescent intensity related to the enzymatic activity of cas-3, **C)** the n-fold increase in fluorescent intensity related to the enzymatic activity of cas-9, **D)** the n-fold increase in fluorescent intensity related to the generation of ROS and

E) the n-fold increase in fluorescent intensity related of RNS in U-251 MG spheroids with no treatment (CTRL), treated with sorafenib (SOR), treated with cell membrane-coated nanocubes (CM-NCubes), treated with sorafenib-loaded cell membrane-coated nanocubes (SOR-CM-NCubes), without or with exposure to an alternating magnetic field (AMF), after 3 consecutive days of exposure (3 h every day); *n* = 3, one-way ANOVA, a detailed statistical analysis is provided in the ESI†.

3. Conclusions

In this work, we synthesized a hybrid nanocube consisting of an inorganic core (Fe_3O_4/MnO_2) coated with a lipid layer extracted from cell membranes, derived from the U-251 MG cell line. These CM-NCubes presented good magnetic properties and NMR relaxation times, thus demonstrating their potential to be used as theranostic agents. Furthermore, the CM-NCubes demonstrated good antioxidant capabilities due to H_2O_2 scavenging that led to a well-controlled and concentration-dependent oxygen generation. For the first time in the scientific literature, we were able to demonstrate an intracellular temperature increment caused by the exothermic reaction between CM-NCubes and H_2O_2, suggesting that it is possible to make use of the intracellular ROS to locally increase temperature and thus, contributing to hyperthermia. Moreover, it was demonstrated that CM-NCubes present a preferential uptake from the homotypic U-251 MG cell line compared to other brain cell lines (C8-D1A, bEnd.3 and SH-SY5Y), as well as that the cell membrane coating significantly increases the internalization of the particles compared to other biocompatible lipid coatings. Using an *in vitro* BBB model it was shown that 75.0 ± 3.7% of the incubated CM-NCubes in the abluminal part of a Transwell© insert is able to pass through after 48 h and to be subsequently internalized by U-251 MG cells. Using an *in vitro* BBB model it was shown that 75.0 ± 3.7% of the incubated CM-NCubes in the abluminal part of a Transwell© insert is able to pass through after 48 h, and to be subsequently internalized by U-251 MG cells. Using an

in vitro dynamic model of the BBB, the possibility to magnetically accumulate CM-NCubes leading to a higher accumulation of the nanostructures from both bEnd.3 and U-251 MG cells was demonstrated. Finally, it was shown that the exposure of U-251 MG spheroids to an AMF for 3 days significantly increases apoptotic and necrotic cells as well as in caspase-9 levels, in the presence of CM-NCubes and SOR-CM-NCubes under the AMF. A higher increase in ROS levels was also observed for the samples treated with CM-NCubes and SOR-CM-NCubes under the influence of the AMF, while no significant increase could be observed in the RNS levels. Although the acquired data are encouraging, we acknowledge the fact that the used models (BBB, 3D spheroids) have limitations, and much further investigation including *in vivo* studies (to elucidate pharmacokinetics, biodistribution, BBB crossing, *in vivo* hyperthermia, and MRI contrast features), are needed before considering the specific system suitable as a realistic theranostic platform for glioblastoma.

4. Experimental section

4.1 Preparation of CM-NCubes

Inorganic Fe_3O_4/MnO_2 nanocubes (NCubes) were synthesized using a modified procedure previously reported in the literature. [29] Briefly, 695 mg (2.5 mmol) of iron sulfate heptahydrate ($FeSO_4 \cdot 7H_2O$) were dissolved in 94 ml of distilled water, inside a 300 ml conical flask, and stirred for 1 h at 300 rpm, while in parallel 39.5 mg (0.25 mmol) of potassium permanganate ($KMnO_4$) were dissolved in 5 ml of distilled water inside a 7 ml plastic vial, by shaking at 100 rpm for 1 h. Then, 1 ml of 5 M sodium hydroxide (NaOH) were added drop by drop using a syringe pump (1 ml min^{-1}) in the iron solution and stirred for 10 min. Thereafter, the temperature was adjusted to 90°C, and while increasing, the potassium solution was added at the same speed as performed for the NaOH. The stirring speed increased to 500

rpm and the solution was left at this temperature for 12 h. Afterward, the solution was left to cool down at room temperature and cleaned three times using distilled water through centrifugation (10 min, 9000 rpm, 4°C). The precipitate was always kept in water and a small aliquot was freeze-dried in order to calculate the concentration of the final product.

In order to prepare cell membrane-coated CM-NCubes, we first extracted the cell membrane from the U-251 MG cell line using a modified procedure from a previously reported method[30]. Briefly, U-251 MG cells were cultured in DMEM with 10% of FBS (Gibco), 1% of penicillin/streptomycin (P/S, Thermo Fisher Scientific) and 1% of L-glutamine (L-glu, Thermo Fisher Scientific) in a humidified environment with 5% CO_2 at 37°C. When cells reached confluence, they were detached from the 10 cm Petri dishes using 0.05% trypsin-EDTA (Thermo Fisher Scientific). The cell dispersion was washed 3 times with Dulbecco's phosphate buffer saline 1× (DPBS, Thermo Fisher Scientific) and re-dispersed in distilled water. The new cell dispersion was transferred to a high-pressure homogenizer (HPH, Emulsiflex B15, Avestin) and the cell membrane was disrupted at a pressure of 6000 psi / 412.5 bar with 10 passages. The disrupted cell-dispersion was centrifuged at 10000 rpm for 10 min to remove debris and non-disrupted cell organelles, and the supernatant was centrifuged again at 60000 g for 90 min. The collected cell membranes were kept at 4°C until further use.

Concerning the coating, 2 mg of NCubes were dispersed in 1 ml of water and sonicated using a Fisherbrand™ Q125 Sonicator (50% amplitude) for 10 min at 4°C. Afterward, 1 ml of the extracted cell membranes (derived from $10 \cdot 10^6$ cells) was mixed with the NCubes dispersion and sonicated for a further 20 min at the same amplitude. Three cleanings with deionized water were carried out by spinning down the samples for 15 min at 16000 g at 4°C.

As a control, the coating of the NCubes was moreover carried out with commercial lipids, by using a modified protocol previously reported by our group.[19] Briefly, 5 mg of dry NCubes were mixed with 6 mg of cetyl palmitate (Gattefosse), 2 mg glycerol monooleate (Sigma Aldrich), 2 mg of methoxy poly (ethylene glycol) (5000 g mol^{-1}) -1,2-distearoyl-sn-glycerol-3-phosphoethanolamine (mPEG-DSPE, DBA Italia), and 200 µl of chloroform ($CHCl_3$, Sigma Aldrich) and sonicated for 20 min at 4°C using a Fisherbrand™ Q125 Sonicator. After the complete dissolution of the lipids and the homogenization with the dry NCubes, 3 ml of pre-warmed (60°C) Tween® 80 solution (1% w/v, Sigma Aldrich) were added to the mixture and sonicated at 50% for 10 min using a Fisherbrand™ Q125 Sonicator. The lipid-coated nanocubes (LP-NCubes) were cleaned 3 times with deionized water by spinning down the samples for 15 min at 16000 g at 4°C.

4.2 Morphological and physicochemical characterization

The morphological characterization of the CM-NCubes was performed using a transmission electron microscope FEI Tecnai G2 F20 TWIN TMP with a Schottky emitter operated at 200 kV. The EDS analyses have been carried out by using a Bruker XFlash 6|T30 silicon-drift detector (SDD), with 30 mm^2 effective area. Each sample has been sonicated for a few minutes to avoid the presence of aggregates. 5 µl of the solution have been dropped onto an ultrathin carbon-coated Cu grid. The samples were stained with 1% uranyl acetate before the TEM analysis.

The analysis of the spheroids was carried out with a FEI 200 scanning electron microscope (SEM) operating at 5-20 keV, with beam currents varying from 43 pA to 0.17 nA. The elemental analysis was performed using a built-in Bruker Nano XFlash 5010 detector. All of the samples were coated with gold at 25 mA for 70 s before analysis. The cross-sections of the samples were performed with the same microscope equipped with a focused ion beam

delivering a 15keV beam of gallium (Ga^+) ions, with beam currents varying between 43 pA to 0.17 nA.

XPS of the nanoparticles was performed with a SPECS instrument equipped with a Phoibos 150 1D-DLD analyzer and with a monochromatized Al Kα (1486.6 eV) radiation source. Survey scans (1400 to 0 eV binding energy -BE-, step energy 1 eV, dwell time 0.1 s, pass energy 80 eV) were acquired with an electron take-off angle of 90°. High-resolution scans (step energy 0.1 eV, dwell time 0.1 s, pass energy 30 eV) were also acquired with an electron take-off angle of 90°. The hydrocarbon peak component in the C 1s spectra was set at 285.0 eV to correct sample charging. The spectrometer was previously calibrated with the peak of Ag 3d 5/2 (368.28 eV).

Infrared spectroscopy was performed using a Shimadzu Miracle 10. Before the measurements, all the samples have been freeze-dried. The number of scans was set to 45, the scanning range was set from 4000 to 400 cm^{-1} and the resolution step at 4 cm^{-1}. The graphs were plotted using Origin Pro software 9.1.

The diffraction patterns of the NCubes and CM-NCubes were obtained using a Phillips X'pert PRO X-ray diffractometer, with theta-theta configuration, under the following conditions: CuKα radiation (λ = 1.5418 Å), scans in the 2θ range of 10-80° with a current of 40 mA, a voltage of 40 kV, and a scan rate of 2.8° min^{-1}.

The thermal degradation of the samples was studied by means of TGA, using a TA Instruments TGA model Q50-0545 in platinum pans, with nitrogen flux of 60 ml min^{-1} for each sample. Samples of approximately 5 mg were heated from room temperature to 600 °C at a heating rate of 10 °C min^{-1}, recording continuously the heat flow, sample temperature, sample weight and its time derivative.

Dynamic light scattering measurements were performed using a Zetasizer NanoZS90, Malvern instruments LTD. The measurements were carried out at 37°C and media with different pH and conductivity (H_2O, DMEM, and aCSF), as well as different supplements (FBS, albumin, transferrin, and ferritin). For the hydrodynamic diameter measurements, the concentration for all the samples was adjusted to 100 µg ml^{-1}. The Z potential measurements were carried out in ultrapure water at pH 5.5 and the conductivity was adjusted in the range 30-100 µS cm^{-1}. The attenuation of the samples during measurement was approximately 9. The size and the surface charge measurements represent the mean ± SD of 3 different measurements and with 17 runs in each measurement. Before each measurement, the samples were sonicated for ~10 s using a Bandelin ultrasonic probe at 8 W, to avoid the presence of aggregates during measurements, except in the case of the 24 h stability study.

ICP-OES was performed using an iCAP 6300 DUO Thermo spectrometer from Thermo Fisher Scientific. All chemical analyses performed by ICP-OES were affected by a systematic error of about 5%. Samples were dissolved in HCl/HNO_3 3:1 (v/v) before measurements.

Mass spectroscopy (MS) was performed using a linear Trap Quadropole Orbitrap Velos Pro MS, coupled with an Ultimate 3000 HPLC. Raw MS files were processed with MaxQuant software version 1.6.6.0. Before the analysis, the samples were solubilized in 50 µl of 2% of sodium deoxycholate (SDC), 40 mM of chloroacetamide, 10 mM of tris(2-carboxyethyl) phosphine) (TCEP) and 100 mM of Tris HCl at pH 8, 100°C for 5 min, and digested with 1 µg of trypsin at 37°C for 3 h. The digested samples were processed using the in-stage tip (iST) protocol. [31]

Concerning magnetic characterization, room temperature magnetic hysteresis loops were recorded by a vibrating sample magnetometer (VSM – 1.2H/CF/HT Oxford Instruments) in a magnetic field range ± 1 T, at room temperature.

The local spin dynamics and the MRI contrast efficiency were assessed by means of ^{1}H Nuclear Magnetic Resonance (NMR) relaxometric characterization. The NMR-dispersion profiles (**Fig. S8-A**, ESI^{+}) were collected at room temperature by measuring the longitudinal and the transverse nuclear relaxation times T_1 and T_2, in the frequency range 10 kHz < ν < 56.7 MHz for T_1 and in the range 3.7 MHz < ν < 56.7 MHz for T_2. A SMARTracer Stelar relaxometer was used to generate and detect the NMR signal in the 10 kHz-9.5 MHz range using the fast-field cycling technique; for the ν > 7 MHz range, a Stelar Spinmaster Fourier transform nuclear magnetic resonance (FT-NMR) spectrometer was employed, while for frequencies ν > 3.7 MHz, non-pre-polarized Saturation Recovery (SR) and Carr Purcell Meiboom Gill (CPMG) pulse sequences were used for T_1 and T_2 measurements, respectively. For frequencies ν <3.7 MHz, pre-polarized Saturation Recovery for T_1 was adopted, and care was taken so that a sufficiently homogeneous magnetic field was present. The NMR relaxometry measurements were performed on CM-NCubes dispersed in milliQ water. NMR results at magnetic fields (frequencies) of 0.2 T (8.5 MHz), 0.5 T (21.3 MHz) and 1.33 T (56.7 MHz) reported in the paper were similar to the ones covered by the clinical imaging systems. The efficiency of the CM-NCubes dispersion in contrasting the magnetic resonance images was estimated according to the usual definition of nuclear relaxivity values r_1 and r_2: $r_{1,2}= [(1/T_{1,2\ NP+water} - 1/T_{1,2\ water})/c]$, where T_1 and T_2 represent the longitudinal and transverse nuclear relaxation times in the presence (NP + water) or absence (water) of CM-NCubes, and *c* is the concentration of the magnetic part of the sample.

The MRI experiments were performed at 8.5 MHz using an Artoscan Imager by Esaote SpA. The employed pulse sequence was an High resolution Spin Echo sequence with TR/TE/NEX = 5000 ms / 120 ms / 1, matrix = 256·192, FOV = 180·180. Here, TE is the echo time, TR the repetition time, and NEX the number of averages. The quantification of the signal intensity was performed using ImageJ, considering as control (100%) the signal of the water.

Magnetic hyperthermia was performed using a MagneTherm^{TM} equipment from NanoTherics limited. The applied alternating magnetic field ranged from 12 to 20 mT and the corresponding frequencies ranged from 177 KHz to 1017 kHz. The samples were placed inside a 2 ml Nalgene tube which subsequently was placed inside a polystyrene case in order to reduce thermal fluctuations. The polystyrene case with the sample was placed inside a round coil, either 9 turns with a diameter of 44 mm (9 turn-44 mm) or 9 turns with a diameter of 56 mm (9 turn-56 mm), and the hyperthermia measurements lasted 2 h. The temperature was recorded every second using an Osensa optical fiber temperature probe.

Oxygen generation was recorded every 1 s using a Microx 4 trace fiber-optic oxygen meter with a PSt7-02 microsensor (PreSens, Germany), while the temperature was recorded every 1 s using an OSENSA single channel optic fiber. Varying amounts of CM-NCubes (200, 500 and 1000 μg ml^{-1}) were placed in a 1.5 ml airtight Eppendorf vials with 0.5 ml of complete medium. Both of the sensors were placed through a hole in the cap and left for 30 min to equilibrate O_2 and temperature levels. Afterward, 0.5 ml of 0, 0.1, 0.5, 1.0 or 2.0 mM H_2O_2 were added in the vial, aiming at having final concentrations of H_2O_2 0, 0.05, 0.25, 0.5 and 1 mM, and final concentrations of CM-NCubes 100, 250 and 500 μg ml^{-1}.

The antioxidant measurements were carried out by using an ABTS Antioxidant Assay Kit by Zen-Bio, Inc. following the manufacturer's instructions. The antioxidant ability of the CM-

NCubes was compared with the antioxidant ability of Trolox (6-Hydroxy-2,5,7,8-tetramethylchroman-2-carboxylic acid), which is a water-soluble analog of vitamin E, known for its strong antioxidant properties.

The drug loading and release studies were performed using an HPLC Shimadzu LC-20AT. The chromatographic separation was carried out using a C-18 column (150 mm × 4.6 mm i.d., 5 µm particle size). The mobile phase consisted of methanol and water (containing acetic acid 1%) and pumped in isocratic mode (80% MeOH- 20% H2O) with a flow rate of 0.5 ml min^{-1}. The elution of the analyte was monitored at 240 nm. The standard curve was prepared by dissolving 5 mg of SOR in 5 ml volume of the mobile phase and filtering using a 0.2 µm syringe filter. A concentration range of 0.1-325 µg ml^{-1} was prepared upon further serial dilution. To calculate the loading capacity after the loading, all the supernatants were collected, filtered and measured using the above conditions. For the release studies, at each time point, the samples were centrifuged at 15000 rpm for 1 h at 4°C and the supernatant of each solution was removed and replaced with a fresh one of the same volume. 20 µl of each supernatant was injected into the HPLC and analyzed using the parameters above described. The SOR peak was observed at 3.8-4.0 min.

For the loading of the CM-NCubes, 500 µg of sorafenib were mixed with 10 mg of NCubes in 2 ml final volume of water and sonicated with a Fisherbrand™ Q125 Sonicator (50% amplitude) for 10 min inside an ice bath. Subsequently, 2 ml of the cell-derived membrane in water (derived from 50 x 10^3cells) were added to the SOR-NCubes dispersion and sonicated for 20 min more, still inside the ice bath. Three cleanings with deionized water were carried out by spinning down the samples for 30 min at 16000 g at 4°C. All the supernatants were collected and analyzed with HPLC.

4.3 In vitro studies

In this study, the glioblastoma multiforme cell line U-251 MG (formerly known as U-373 ATCC® HTB-17™), the neuroblastoma cell line SH-SY5Y (ATCC® CRL-2266™), the C8-D1A cells [Astrocyte type I clone] (ATCC® CRL-2541™), and the bEnd.3 cells [BEND3] (ATCC® CRL-2299™) were used. U-251 MG, C8-D1A and bEnd.3 cells were cultured in T75 flasks using high glucose DMEM supplemented with 10% FBS, 1% P/S and 1% L-glu, and at normal culture conditions (37°C, 5% CO_2), while SH-SY5Y were cultured in DMEM:F12 (1:1) supplemented with 10% FBS, 1% P/S and 1% L-glu at the same conditions as the other cell lines. For all the experiments the used cells were between passage 10 and passage 20. The medium during culture was changed every two days.

For the intracellular temperature studies, U-251 MG cells were seeded at a concentration of 25000 cm^{-2}, using a complete medium containing 25 mM (4-(2-hydroxyethyl)-1-piperazine ethanesulfonic acid, HEPES) in a Willco well (GWST-3512) with a glass bottom, and incubated at cell culture conditions overnight. After 24 h, half of the samples were treated with 250 µg ml^{-1} (treated sample) of CM-NCubes and left again for 24h in order to allow the nanostructures to be internalized by the cells. After 24 h, untreated and treated samples were stained using ER Thermo Yellow (300 nM for 30 min at 37°C), a fluorescent temperature sensitive dye. The time-lapse fluorescence imaging was then performed by using a Nikon C2+ confocal laser microscope equipped with a 60× oil objective and by taking advantage of the automated focal control through the Nikon Perfect Focus System. Subsequently, the medium loaded with the fluorescent dye was discharged and replaced with the solution for imaging, which consisted of phenol red-free DMEM supplemented with 25mM of HEPES. The samples were left for 1 h at room temperature in order to equilibrate the temperature, and then the excess media was removed, leaving only 100 µl in the Willco dish. Fluorescence intensities

($\lambda_{ex/em}$ = 561/570<λ_{em}<1000 nm) were recorded every 10 s during the gentle addition of 20 µl of media containing a predetermined concentration of H_2O_2, and for 3 min after the addition of the media. Finally, fluorescence intensities were converted to temperature levels by following a calibration (3.9% decrement fluorescence °C^{-1}) as reported elsewhere.[25a]

To evaluate the ability of the CM-NCubes to be internalized by cells typical of the BBB as well as by glioblastoma cells, and additionally to assess their ability to specifically target the homotypic U-251 MG cell line, we performed flow cytometry and confocal microscopy studies at two different time points (4 and 24 h), using four different cell lines (U-251 MG, SH-SY5Y, C8-D1A and bEnd.3), and two different coatings (cell membrane and commercial lipids coating). For the flow cytometry studies, the various types of cells were seeded in 24-wells plate (Corning®) in triplicate at a density of 25000 cells cm^{-2}, 24 h before the nanoparticle treatment. After 24 h the media were changed with media containing 10 µg ml^{-1} of (3-octadecyl-2-[3-(3-octadecyl-2(3H)-benzoxazolylidene)-1-propenyl]-, perchlorate) (DiO) (Thermo Fisher) stained particles, and at predetermined time points the supernatant was removed and a gentle wash with DPBS for 3 times followed. Then, the cells were detached using 0.05 % trypsin-EDTA. Cells were centrifuged at 1500 rpm for 5 min and the pellet was gently re-dispersed in DPBS 1×. For the confocal studies, the various types of cells were seeded in 24-well plates with black walls and flat and clear bottom (Ibidi®) in triplicate at a density of 25000 cells cm^{-2}, 24 h prior the nanoparticle treatment. After 24 h the media was changed with media containing 100 µg ml^{-1} of CM-NCubes and LP-NCubes and at predetermined time points the cells were washed three times with DPBS 1× and then fixed for 20 min at 4°C with paraformaldehyde (PFA, Sigma Aldrich, 4% in DPBS 1×). After the fixation, the cells were incubated for 30 min at room temperature with a blocking solution of goat serum (10% in DPBS 1×) and then stained for 30 min at 37°C with a solution containing

TRITC-phalloidin 0.165 µM (Sigma Aldrich) and Hoechst 5 µg ml^{-1} (Invitrogen). After staining, the cells were washed two times with DPBS 1×. The internalization of the CM- and LP-NCubes by the different cell lines was studied using flow cytometry (CM-NCubes in green $\lambda_{ex/em}$= 488/525 nm) and confocal laser scanning microscopy on a Nikon C2+ system (actin filament in red $\lambda_{ex/em}$= 561/585 nm, CM-NCubes in white, nuclei in blue $\lambda_{ex/em}$=401/447 nm). For the flow cytometry studies the CM-NCubes were stained with the DiO dye, the excitation and emission wavelengths of which are described above, while for the internalization studies using confocal microscopy unstained CM-NCubes were detected at the wavelength of 647 nm.

U-251 MG spheroids were formed following a modified protocol previously reported in the literature.[32] Briefly, each well of a 48-multiwell plate (Corning®) was covered with 100 µl of hot agarose solution in DPBS 1× (15 mg ml^{-1}) and left for 30 min at room temperature to cool down. Afterwards, 1 ml of complete DMEM containing $100 \cdot 10^3$ U-251 MG cells was added in each well. The multi-wells were incubated at 37°C and at 5% CO_2 until the spheroids were completely formed at day 7. The medium was not changed until the end of the experiment, aiming at the creation of a hypoxic and low pH environment that simulates the tumor microenvironment. U-251 MG spheroids were characterized using optical microscopy (**Fig. S12**, ESI†), while plain spheroids and CM-NCubes treated spheroids were also characterized using scanning electron microscopy and energy dispersive X-ray analysis (**Fig. S13**, ESI†). Cross-section images using focused ion beam microscopy were also performed aiming at confirming the internalization of the particles by the spheroids (**Fig. S14**, ESI†).

Apoptosis and cell proliferation on the U-251 MG spheroids were assessed using the annexin V-FITC/PI (Thermo Fisher Scientific) assay as per manufacturer instructions.

At day 2 of the growing U-251 MG spheroids (in complete media containing HEPES), 500 μg ml^{-1} of the SOR-CM-NCubes and the corresponding free sorafenib (10 μg ml^{-1}) were added to the 48-multiwell containing the spheroids. Both the particles and the free drug were incubated 2 days before the initiation of the spheroid exposure to the alternating magnetic field, that lasted further 3 days. At day 5, the supernatant was removed, and the spheroids were transferred into 2 ml Nalgene vials with fresh complete media containing HEPES; each vial contained 5 spheroids and a volume of 500 μl.

Samples treated with sorafenib (SOR), cell membrane-coated nanocubes (CM-NCubes), sorafenib-loaded cell membrane nanocubes (SOR-CM-NCubes) and untreated samples were exposed to an AMF for 3 h per day for 3 days. For each of the above samples, a Nalgene tube with the same number of spheroids and the same treatment was kept in a water bath at 37°C for 3 h without any exposure to the AMF. At day 8, the spheroids from each Nalgene tube were broken into single cells by pipetting and incubated with annexin V-FITC/PI following the manufacturer's protocols. Cells stained with annexin V-FITC/PI were evaluated using a Beckman Coulter cytoflex. Live cells (Annexin V- / PI-), early apoptotic cells (Annexin V+ / PI-), late apoptotic cells (Annexin V+ / PI+) and necrotic cells (Annexin V- / PI+) were analyzed using the Cytoflex software (Beckman Coulter). Unstained cells with and without particles were used as controls.

Caspase-3 and caspase-9 enzymatic activity were assessed using CaspGLOW^{TM} Fluorescein Active assay kits (Thermo Fisher Scientific) following the manufacturer’s protocol. The samples and the applied treatments are described in the assessment of apoptosis and cell proliferation paragraph.

The generation of reactive oxygen and nitric oxide in the samples that underwent various treatments (see assessment of apoptosis and cell proliferation paragraph) was evaluated using the CellROX® Green Reagent (Thermo Fisher Scientific) and the (4-Amino-5-Methylamino-2',7'-Difluorofluorescein Diacetate) (DAF-FM Diacetate) (Thermo Fisher Scientific) dyes following the manufacturer's protocols.

To assess the ability to guide the CM-NCubes across the BBB and towards the glioblastoma site using a static magnetic field, an *in vitro* fluidic model of the BBB [14] was used. The fluidic model consisted of two parallel channels (top and bottom channel) that were separated by a porous membrane, derived from 6 well falcon transwell inserts (3 μm pore size). After coating with gelatin 1%, the upper channel was seeded with 10^5 bEnd.3 cells, while the lower channel was seeded with 10^5 U-251 MG cells, that were left to grow for 5 days (culture conditions were the same as aforementioned for the other experiments). After 5 days of culture, the upper channel was placed under flow using an Ibidi® pump system with a flow rate of 12 ml min^{-1}, of phenol red-free fully complemented cell culture medium (DMEM high glucose 10% FBS) containing 20 μg ml^{-1} of DiO-stained CM-NCubes. The accumulation of the CM-NCubes was achieved in the presence of a static magnetic field (13 mm diameter, 10 mm width, grade N35 NdFeB, axial magnetization) positioned under the device for 2 min, and was thereafter evaluated through confocal imaging. The distribution of the CM-NCubes on the porous membrane of the dynamic BBB model was predicted by using the numerical model described in our previous study. [14] In particular, using the Matlab environment, we derived the sought distribution by numerically integrating the trajectories of nearly 1.25 million CM-NCubes released in the fluid stream and responding to the magnet field as point dipoles. [33] Relevant details are reported in the supporting information. The evaluation of the cellular internalization and the crossing ability of CM-NCubes were evaluated with a

similar approach. A 5 μg ml^{-1} dispersion of DiO-stained CM-NCubes was pumped inside the upper channel of the system, with and without the presence of a static magnetic field at the aforementioned time (2 min) and flow rate. After 2 min, the systems used for the targeting experiment were disconnected from the pump and left in a static condition. After 72 h, bEnd.3 cells in the upper channel and U-251 MG cells in the lower one, in the presence of DiO-stained CM-NCubes, were fixed and stained with TRITC phalloidin and Hoechst (see the previous section for methodological details about fixation and staining), and were evaluated through confocal microscopy.

4.4 Statistical Analysis

The results were presented as mean ± standard deviation. Analyses comparing means of different treatment groups were performed using one-way ANOVA test (GraphPad Prism 7; GraphPad Software, Inc.), corrected for multiple comparisons by the Bonferroni method. Adjusted *p*-values lower than 0.05 were considered significant.

Acknowledgments

This project has received funding from the European Research Council (ERC) under the European Union's Horizon 2020 research and innovation program (grant agreement N°709613, SLaMM).

We would like to kindly thank Dr. Satoshi Arai, Dr. Young-Tae Chang and Dr. Madoka Suzuki for providing the intracellular temperature sensor used for analyzing the temperature increment during the exothermic reaction between the CM-NCubes and hydrogen peroxide. SGIker technical services (UPV/EHU) are gratefully acknowledged for XRD and XPS support.

The authors would like finally to acknowledge also the contribution of the COST Action MyWAVE CA17115 and the COST Action EURELAX CA15209.

References

[1] a) G. S. Stoyanov, D. L. Dzhenkov, M. Kitanova, I. S. Donev, P. Ghenev, *Cureus* **2017**, 9, e1396; b) M. Li, Z. Luo, Z. Xia, X. Shen, K. Cai, *Mater Horiz.* **2017**, 4, 977.

[2] W. Zhu, Z. Dong, T. Fu, J. Liu, Q. Chen, Y. Li, R. Zhu, L. Xu, Z. Liu, *Adv. Funct. Mater.* **2016**, 26, 5490.

[3] A. Bhowmik, R. Khan, M. K. Ghosh, *Biomed. Res. Int.* **2015**, 2015, 320941.

[4] a) G. G. Genchi, A. Marino, C. Tapeinos, G. Ciofani, *Front. Bioeng. Biotechnol.* **2017**, 5, 80; b) C. Tapeinos, E. K. Efthimiadou, N. Boukos, G. Kordas, *Colloids Surf. B* **2016**, 148, 95; c) H. Y. Yang, Y. Li, D. S. Lee, *Adv. Ther.* **2018**, 1.

[5] C. Tapeinos, in *Smart nanoparticles for biomedicine*, DOI: 10.1016/b978-0-12-814156-4.00009-4 **2018**, p. 131.

[6] a) J. Bizeau, C. Tapeinos, C. Marella, A. Larranaga, A. Pandit, *Colloids Surf. B* **2017**, 159, 30; b) D. R. Pereira, C. Tapeinos, A. L. Rebelo, J. M. Oliveira, R. L. Reis, A. Pandit, *Adv. Biosyst.* **2018**, 2; c) P. Prasad, C. R. Gordijo, A. Z. Abbasi, A. Maeda, A. Ip, A. M. Rauth, R. S. DaCosta, X. Y. Wu, *ACS Nano* **2014**, 8, 3202; d) M. Song, T. Liu, C. Shi, X. Zhang, X. Chen, *ACS Nano* **2016**, 10, 633; e) C. Tapeinos, A. Larranaga, J. R. Sarasua, A. Pandit, *Nanomedicine* **2018**, 14, 2397.

[7] V. Sosa, T. Moline, R. Somoza, R. Paciucci, H. Kondoh, L. L. ME, *Ageing Res. Rev.* **2013**, 12, 376.

[8] a) G. Y. Liou, P. Storz, *Free Radic. Res.* **2010**, 44, 479; b) B. Muz, P. de la Puente, F. Azab, A. K. Azab, *Hypoxia (Auckl)* **2015**, 3, 83; c) E. B. Rankin, A. J. Giaccia, *Science* **2016**, 352, 175; d) N. Rohwer, T. Cramer, *Drug Resist. Updat.* **2011**, 14, 191.

[9] a) Y. Jo, E. H. Kim, S. Sai, J. S. Kim, J. M. Cho, H. Kim, J. H. Baek, J. Y. Kim, S. G. Hwang, M. Yoon, *Int. J. Mol. Sci.* **2018**, 19; b) P. L. Nghiemphu, V. A. Ebiana, P. Wen, M. Gilbert, L. E. Abrey, F. Lieberman, L. M. DeAngelis, H. I. Robins, W. K. A. Yung, S. Chang, J. Drappatz, M. P. Mehta, V. A. Levin, K. Aldape, J. E. Dancey, J. J. Wright, M. Prados, J. Kuhn, T. F. Cloughesy, *J. Neurooncol.* **2018**, 136, 79; c) D. A. Reardon, J. J. Vredenburgh, A. Desjardins, K. Peters, S. Gururangan, J. H. Sampson, J. Marcello, J. E. Herndon, R. E. McLendon, D. Janney, A. H. Friedman, D. D. Bigner, H. S. Friedman, *J. Neurooncol.* **2011**, 101, 57.

[10] C. Saraiva, C. Praca, R. Ferreira, T. Santos, L. Ferreira, L. Bernardino, *J. Control Release* **2016**, 235, 34.

[11] H. H. Gustafson, D. Holt-Casper, D. W. Grainger, H. Ghandehari, *Nano Today* **2015**, 10, 487.

[12] a) J. Y. Zhu, D. W. Zheng, M. K. Zhang, W. Y. Yu, W. X. Qiu, J. J. Hu, J. Feng, X. Z. Zhang, *Nano Lett.* **2016**, 16, 5895; b) D. Wang, H. Dong, M. Li, Y. Cao, F. Yang, K. Zhang, W. Dai, C. Wang, X. Zhang, *ACS Nano* **2018**, DOI: 10.1021/acsnano.7b08355.

[13] M. Basini, A. Guerrini, M. Cobianchi, F. Orsini, D. Bettega, M. Avolio, C. Innocenti, C. Sangregorio, A. Lascialfari, P. Arosio, *J Alloy Compd* **2019**, 770, 58.

[14] A. Grillone, M. Battaglini, S. Moscato, L. Mattii, C. de Julian Fernandez, A. Scarpellini, M. Giorgi, E. Sinibaldi, G. Ciofani, *Nanomedicine (Lond)* **2019**, 14, 727.

[15] Z. Shu, S. Wang, *J Nanomater* **2009**, 2009, 1.

[16] T. Yamashita, P. Hayes, *Appl. Surf. Sci.* **2008**, 254, 2441.

[17] T. M. Johanns, J. A. Bowman-Kirigin, C. Liu, G. P. Dunn, *Neurosurgery* **2017**, 64, 165.

[18] a) J. N. Adkins, S. M. Varnum, K. J. Auberry, R. J. Moore, N. H. Angell, R. D. Smith, D. L. Springer, J. G. Pounds, *Mol. Cell Proteomics* **2002**, 1, 947; b) A. V. Bleicher, H. W. Unger, S. J. Rogerson, E. H. Aitken, *MethodsX* **2018**, 5, 648.

[19] C. Tapeinos, A. Marino, M. Battaglini, S. Migliorin, R. Brescia, A. Scarpellini, C. De Julian Fernandez, M. Prato, F. Drago, G. Ciofani, *Nanoscale* **2018**, DOI: 10.1039/c8nr05520c.
[20] J. T. Jang, J. Lee, J. Seon, E. Ju, M. Kim, Y. I. Kim, M. G. Kim, Y. Takemura, A. S. Arbab, K. W. Kang, K. H. Park, S. H. Paek, S. Bae, *Adv. Mater.* **2018**, 30.
[21] W. J. Atkinson, I. A. Brezovich, D. P. Chakraborty, *IEEE Trans. Biomed. Eng.* **1984**, 31, 70.
[22] K. Simeonidis, M. P. Morales, M. Marciello, M. Angelakeris, P. de la Presa, A. Lazaro-Carrillo, A. Tabero, A. Villanueva, O. Chubykalo-Fesenko, D. Serantes, *Sci. Rep.* **2016**, 6, 38382.
[23] Z. R. Stephen, F. M. Kievit, M. Zhang, *Materials Today* **2011**, 14, 330.
[24] Y. Grosu, A. Faik, I. Ortega-Fernández, B. D'Aguanno, *Sol. Energ. Mat. Sol. C.* **2017**, 161, 170.
[25] a) S. Arai, S. C. Lee, D. Zhai, M. Suzuki, Y. T. Chang, *Sci Rep* **2014**, 4, 6701; b) A. Marino, S. Arai, Y. Hou, A. Degl'Innocenti, V. Cappello, B. Mazzolai, Y. T. Chang, V. Mattoli, M. Suzuki, G. Ciofani, *ACS Nano* **2017**, 11, 2494.
[26] M. Battaglini, C. Tapeinos, I. Cavaliere, A. Marino, A. Ancona, N. Garino, V. Cauda, F. Palazon, D. Debellis, G. Ciofani, *ACS Biomater. Sci. Eng.* **2018**, DOI: 10.1021/acsbiomaterials.8b01033.
[27] A. Rodriguez-Hernandez, E. Navarro-Villaran, R. Gonzalez, S. Pereira, L. B. Soriano-De Castro, A. Sarrias-Gimenez, L. Barrera-Pulido, J. M. Alamo-Martinez, A. Serrablo-Requejo, G. Blanco-Fernandez, A. Nogales-Munoz, A. Gila-Bohorquez, D. Pacheco, M. A. Torres-Nieto, J. Serrano-Diaz-Canedo, G. Suarez-Artacho, C. Bernal-Bellido, L. M. Marin-Gomez, J. A. Barcena, M. A. Gomez-Bravo, C. A. Padilla, F. J. Padillo, J. Muntane, *Redox Biol.* **2015**, 6, 174.
[28] A. Tomitaka, T. Yamada, Y. Takemura, *J Nanomater.* **2012**, 2012, 1.
[29] X. Liu, N. Wu, C. Cui, N. Bi, Y. Sun, *RSC Advances* **2015**, 5, 24016.
[30] C. Gao, Z. Lin, B. Jurado-Sanchez, X. Lin, Z. Wu, Q. He, *Small* **2016**, 12, 4056.
[31] N. A. Kulak, G. Pichler, I. Paron, N. Nagaraj, M. Mann, *Nat Methods* **2014**, 11, 319.
[32] J. Friedrich, C. Seidel, R. Ebner, L. A. Kunz-Schughart, *Nat. Protoc.* **2009**, 4, 309.
[33] L. C. Berselli, P. Miloro, A. Menciassi, E. Sinibaldi, *Appl. Math. Comput.* **2013**, 219, 5717.